Interpreting the distributions of absorbed dose in an incompletely zeroed natural luminescent dosimeter

Joanna Baran

Department of Radioisotopes
Institute of Physics, Silesian University of Technology

M.Sc. thesis
November 13th, 2002.

Table of contents

1 Acknowledgements

First of all, I would like to thank Dr. Andrzej Bluszcz for being my supervisor during my individual studies at the Department of Radioisotopes, the Institute of Physics, Silesian University of Technology. I also wish greatly to thank Dr. Andrew Murray of the Nordic Laboratory for Luminescence Dating (NLL) for invaluable aid and supervision during the Jönköping project of which he was in charge, and Dr. Lars Bøtter-Jensen for giving me the possibility of spending 8 months of practice at the Risø National Laboratory on a Leonardo da Vinci scholarship. I would further like to thank Mr. Leif Häggström for providing the samples, which formed the basis of this work. And last but not least I wish to thank all the staff from NLL, Risø National Laboratory and from the Silesian University of Technology for the time spent on helping me out and introducing me to the techniques used in their laboratories as well as for giving me the possibility to use them. In particular, I wish to thank Mette Adrian and Anne Sørensen, NLL, for their kindness and help.

I finally wish to send my most sincere gratitude to my family for giving me strength, hope and financial support, and greetings to all the people whom I have met during my five years of studying in Poland as well as in Denmark.

2 Aim and scope of the thesis

2.1 Aims

This thesis describes the use of luminescence dating techniques to date sediment from within stone structures. Stone structures are in general rather difficult to date using radiocarbon due to the lack of associated organic material. Using luminescence dating methods, however, one may in principle obtain a direct measurement of the time elapsed from the last natural exposure to light of an associated sediment, to the present day. This is because the last exposure to light removes any prior natural luminescence signal. Hence, this method could prove to be a valuable tool in future archaeological applications.

In this thesis, I aim to demonstrate the applicability of luminescence dating techniques to the dating of stone structures in an archaeological context. For this purpose I have studied material derived from an archaeological site in Sweden, including: sediment infill from between the stones in a wall and a clearance cairn; soil samples taken beneath these structures; two sandy samples from a hearth (above and below); and two heated stones, taken from inside the wall and from the hearth, respectively. Two luminescence techniques were used for these studies, the Single Aliquot Regenerative dose method and the Single Grain Regenerative dose method, and the results are compared.

2.2 Contents

The main material in this thesis has been divided into four parts, represented consecutively by the main Chapters 4 through 7. A short introduction will be found in Chapter 3, while an overall discussion of the results is presented in the concluding Chapter 8. A discussion of the aims and scope of the work is to be found in the present chapter as well as this overview of its contents.

The introductory Chapter 3 contains basic information about the archaeological site in Sweden studied in this thesis, including a summary of existing dating techniques and their application at the Öggestorp site. Samples taken from the site are also listed.

Chapter 4 provides a general discussion of the Optically Stimulated Luminescence (OSL) process as well as the OSL techniques used in this work. This includes the results of testing and calibration of the Risø OSL reader as well as of the sampling material. These test measurements were necessary in order to be able to select the best conditions for measuring the apparent equivalent dose, D_e of the sediment samples and for selecting the optimum grain size for measurements. Also, they provide an integral check of the instrument itself.

Chapter 5 presents the results of measuring dose distributions in unheated materials and reports on OSL measurements using the Single Aliquot Regenerative dose and Single Grain Regenerative dose techniques, respectively. The chapter is divided into three main sections; the first two sections discussing the results obtained using the two different methods, while the last section compares the results.

Chapter 6 contains a discussion of results obtained using samples of heated stone. The samples discussed in this chapter were measured using the single aliquot technique. Samples from two different heated stones were processed, one of which was found inside the wall, the second coming from a hearth. Both cases prove to yield good examples of credible ages and can be regarded as providing some age control for the age of the sediments inside, and soil beneath, the stone structures.

Chapter 7 contains an introduction to the high-resolution gamma spectroscopy techniques used here, and reports on the results found from dose rate measurements. It also includes a discussion of the age equation. Knowing the amount of radioactivity is and essential part of OSL dating. Tables found in this chapter include information on the level of radioactivity of various radionuclides, and the derived dry beta and gamma dose rates, and the total dose rates. The tables presented here were used in converting measured doses to ages.

Finally, Chapter 8 presents a comprehensive discussion of the overall results, and draws conclusions on using the Single Aliquot and Single Grain techniques to investigate samples from stone structures. The discussion includes a summary of the results presented in Chapters 4 through 7. Some perspectives are discussed.

A list of references and a short appendix discussing the chemical preparation of OSL samples is also attached.

Joanna Baran. November 2002.

3 Introduction

This thesis reports on the potential of using Optically Stimulated Luminescence (OSL) techniques to determine the construction age of various stone structures at an archaeological site at Öggestorp, near Jönköping in southern Sweden. The stone structures have proved very difficult to date directly, since no or little organic material is in general associated with stone structures. Even when organic material is found, there is no guarantee that it is contemporary. Luminescence studies of natural sediments, however, allow for the dating of a different class of material. The event dated is the last exposure of sediment grains to light; the light exposure removes any prior luminescence signal, effectively zeroing the grains. However, some grains are found to be incompletely zeroed. In these cases only the smallest doses measured are likely to reflect the archaeological age.

When a prehistoric stone structure was built, there was always likely to be some sediment attached to the surfaces of the stone. These sediment grains would have been light exposed during construction; after construction, wind and rain would have immediately begun to emplace these and new light-exposed sediment grains as infill in the interstices of the structure. After these bleaching events, all the light-exposed and unexposed grains would begin to accumulate a further radiation dose proportional to the time elapsed since the construction. In this thesis, the dose distributions from such sediments inside stone structure samples have been studied using both single aliquots and individual grains of quartz. Additionally, results were obtained from studying soil samples just below stone structures. Some of the mineral grains in soil surfaces are continually being exposed to daylight by the actions of soil fauna and flora (e.g. worm casts, emergence of young plants, tree fall). These processes are active until the overlying structures are built, after which the buried surface is protected from further light exposure and begins to accumulate a new radiation dose. The dose distribution from such soil samples have been studied using single aliquots of quartz (grains).

The preliminary construction ages for a stone wall and clearance cairn based on the measured dose distributions have also been compared to independent age constraints derived from OSL ages of associated heated stones (inside the wall and the hearth) and wind blown sand on the hearth. They were also compared to other archaeological evidence.

The table below summarizes the most important dating methods used in modern archaeology. Almost all these methods are based on the comparison with artefacts found in the same place and such association is not always reliable. Also shown in the table are the results of their application at the Öggestorp site:

Method	Principle	Problem	Application in Öggestorp
Comparison with agricultural features of known age.	By comparing features with features of known age in other regions, a probable date can be established.	The age differs between regions.	Clearance cairns can be from 1000 BC to AD 1800. Walls are unknown in the region. Walls from other regions date to 500 BC – AD 500.
Connecting the agricultural remains to other elements nearby.	Graves etc. of known age nearby are used to date the agricultural remains.	A landscape is the accumulative result of thousands of years of activity. The element might not be of the same age as the agricultural feature.	The agricultural remains are close to the graves, but do not overlap them, indicating that they are from the same period (1500 BC – AD 500), or slightly younger.
Landscape stratigraphy.	Landscape stratigraphy gives a relative age of the remains.	It can be hard to identify the stratigraphy.	Some, obviously late-historical, clearance cairns in the south part of the area lie on top of graves.
Land survey maps.	Old land survey maps (usually from the eighteenth and nineteenth centuries) can tell how the area was used in historical time.	An area used in historical time was probably used in prehistorical time as well.	The northern part of the area was used for grazing (with swidden) and the southern for cultivation in historical time.
Artefacts found	Artefacts found in connection to agricultural remains can give a hint of/ about the dating	The problem is to argue that the artefacts found have anything to do with the agricultural remains.	Parts of iron furnaces were found in cairns in the south part of the area. Probably an indication of a clearing or deep ploughing in historical time.
Stratigraphy inside features.	Stratigraphy inside agricultural remains can tell how it was created. The details of the construction of the remains can give a hint of the age.	There are regional and local differences.	Some of the cairns in the southern part lie on top of graves as well as historically cultivated soil.
Radiocarbon	Radiocarbon dating of charcoal may indicate the age of agricultural features	The main problem is to determine the association of the charcoal with the agricultural features. Usually a large number of radiocarbon dates are	The wall, two cairns and two graves were dated to AD 1300 1800, although the graves are in fact obviously older (0 – AD 500). The charcoal is probably a result of the grazing

Method	Principle	Problem	Application in Öggestorp
		taken in order to provide a statistical reliable picture.	and swidden activity in historical time.
Pollen stratigraphy	Pollen stratigraphy from peatbogs near the agricultural features may give an indication of the development of the cultural landscape in the area and also give an indication of when the agricultural features were likely to have been in use (pollen samples can also be taken inside features).	The main problem is how big an area the pollen stratigraphy represents. Another problem is the dating of peatbog cores. The main problem with earthbound pollen is preservation.	A core taken 1 km away shows that pollen from cereal first appears in the period 400 BC – AD 500.

Table 1: Methods of modern archaeology in Sweden with applications at the Öggestorp site (based on Häggström, private communication).

3.1 Archaeological finds at Öggestorp

Öggestorp lies at the border of the south Swedish highlands, approx. 200 metres above sea level. The prehistoric remains in the area are clustered in the gap between two lakes and have had to be excavated due to imminent road construction. The archaeological remains are dominated by a dozen graves dating from the Bronze Age to the Early Iron Age (1500 BC – AD 500) and agricultural features of uncertain age; these include a wall and about 60 clearance cairns. At least one prehistoric settlement has been identified in the area and remains of iron production and a pitway have also been found. About 40 radiocarbon dates from various locations in the vicinity suggests that the most important time in the prehistory of Öggestorp was between 500 BC and AD 500. This is supported by the findings of various Roman artefacts.

Clearance cairns in the region can equally well be from 1000 BC or AD 1800. The wall has no similarity to any other local structure, although to the north-east similar walls date to between 500 BC and AD 500. The agricultural remains (wall and cairns) are close to, but avoid, the grave sites indicating that they are from the same period or slightly younger. Old land survey maps indicate that the northern part of the area has not been used for anything but swidden (slash-and-burn) grazing in historical times. The southern part of the site was in use on the first maps and is still in use. Radiocarbon ages from the agricultural features at the site, however, are of uncertain value. Charcoal from the wall and two cairns yield dates between the fourteenth and eighteenth centuries, as do two dates

from two graves which should be between AD 0 and AD 500. According to Häggström (private communication), these anomalously young radiocarbon ages might be explained by the use of fire in historical times to stimulate the growth of grass for grazing.

3.2 Samples from Öggestorp

Five sediment samples were taken from four different cross-sections of the wall (02 – section #1, 04 – section #2, 07 – section #3 and 09 – section #4 in Figure 3.1) and through a clearance cairn (11 in Figure 3.1). The samples were taken from a central location in each cross-section, a few centimetres above the old soil surface buried by the construction of the wall or cairn. An aeolian sand layer was also sampled immediately above the hearth (12 in Figure 3.1), and a sediment infill sample was taken from the ruins of a brick building in the neighbourhood, demolished within the last 10 years, as a modern analogue.

Five samples of soil beneath a stone structure (01 – section #1, 03 – section #2, 06 – section #3, 08 – section #4 in Figure 3.1) were taken from four different places of the wall – in the same part of it as the sediment samples - and from a clearance cairn (10 in Figure 3.1). The samples were taken from a central location just beneath a wall structure. This was the old soil surface buried by the human activity. Sand immediately above and below the hearth (12, 14 in Figure 3.1) was also sampled. Finally, topsoil samples were taken from a modern soil surface in an adjacent wood. Sand-sized quartz grains were chemically extracted (Appendix A), with only samples 03 and 10 of the quartz extracts giving a significant infra-red stimulated luminescence signal (implying the presence of feldspar contamination)

3.3 Notation

Throughout this thesis the standard uncertainties of the measured values will be given in the form of two decimal digits in brackets following immediately the value. For example a value of 1.33 s with a standard uncertainty of 0.22 s will be written as 1.33(22) s. The digits in the brackets correspond to the uncertainty on the same number of last decimal digits in the given value.

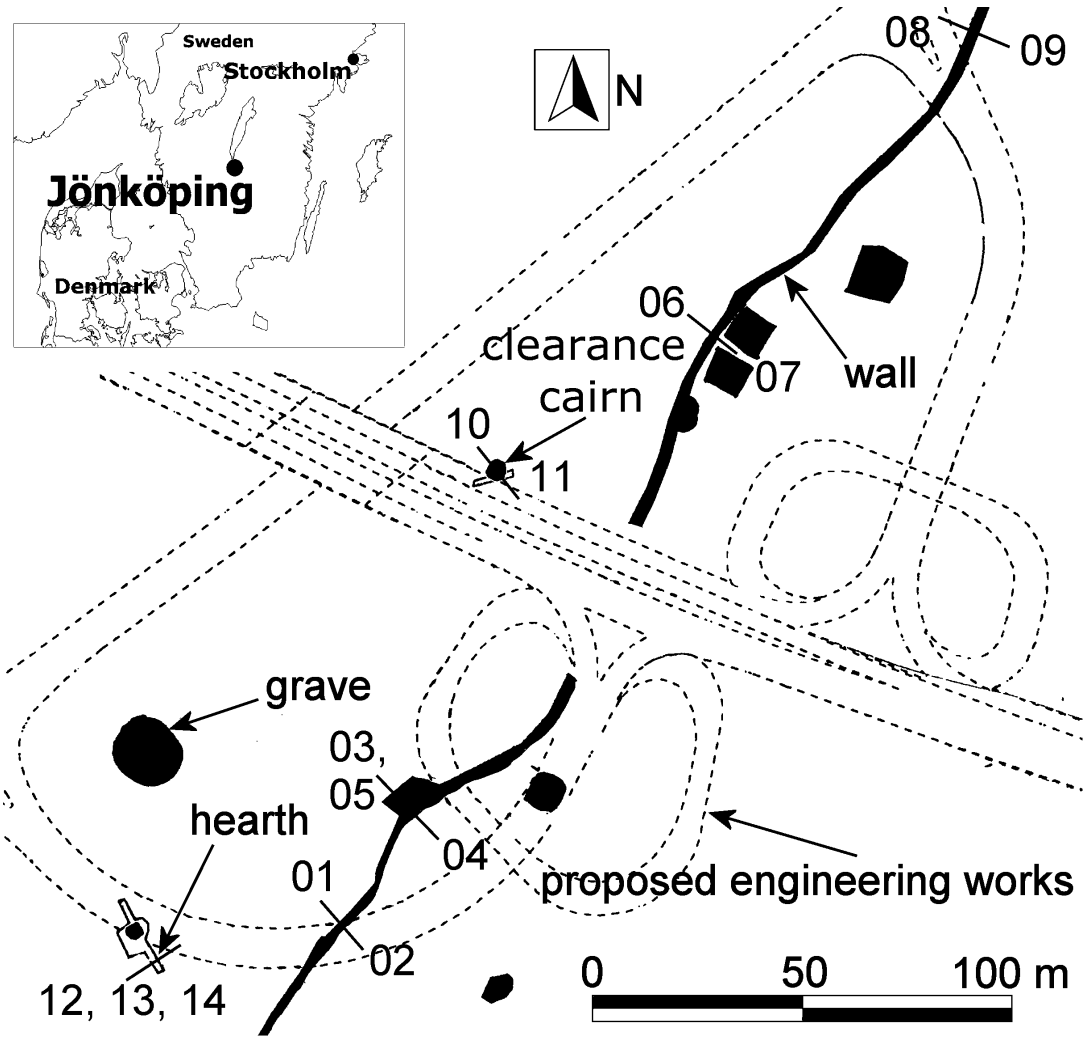

Figure 3.1: Schematic map of the Öggestorp site.

4 OSL techniques and calibration

This chapter discusses the Single Aliquot Regenerative dose (SAR) and Single Grain Regenerative dose methods. A series of test and calibration measurements are also described; these were used to test the performance of the OSL readers as well as to determine appropriate measurement parameters. For the SAR measurements, sediments inside and beneath stone structures were used for these tests, as well as some modern analogues.

4.1 The Optically Stimulated Luminescence (OSL) process

"Luminescence" is when light is emitted by a material stimulated by various external means. Materials showing luminescence properties are called phosphors. The phenomenon is in general divided into phosphorescence and fluorescence. Fluorescence is the emission of light by a material being stimulated by an external source. After removing the stimulation, the luminescence also disappears; fluorescence takes place in less than 10^{-8} s. Phosphorescence on the other hand is present both during and after the end of the stimulation; after removal of the external source the characteristic luminescence decay time is greater than 10^{-8} s.

Defects in the crystal lattice may provide traps for electrons from the conduction band and holes from the valence band, because they can give rise to local permissible energy levels between the conduction band and the valence band. The depths of the electron traps are given by the excitation energy needed to restore electrons to the conduction band. A schematic illustration of this system of ionisation and electron trapping is shown on Figure 4.1.

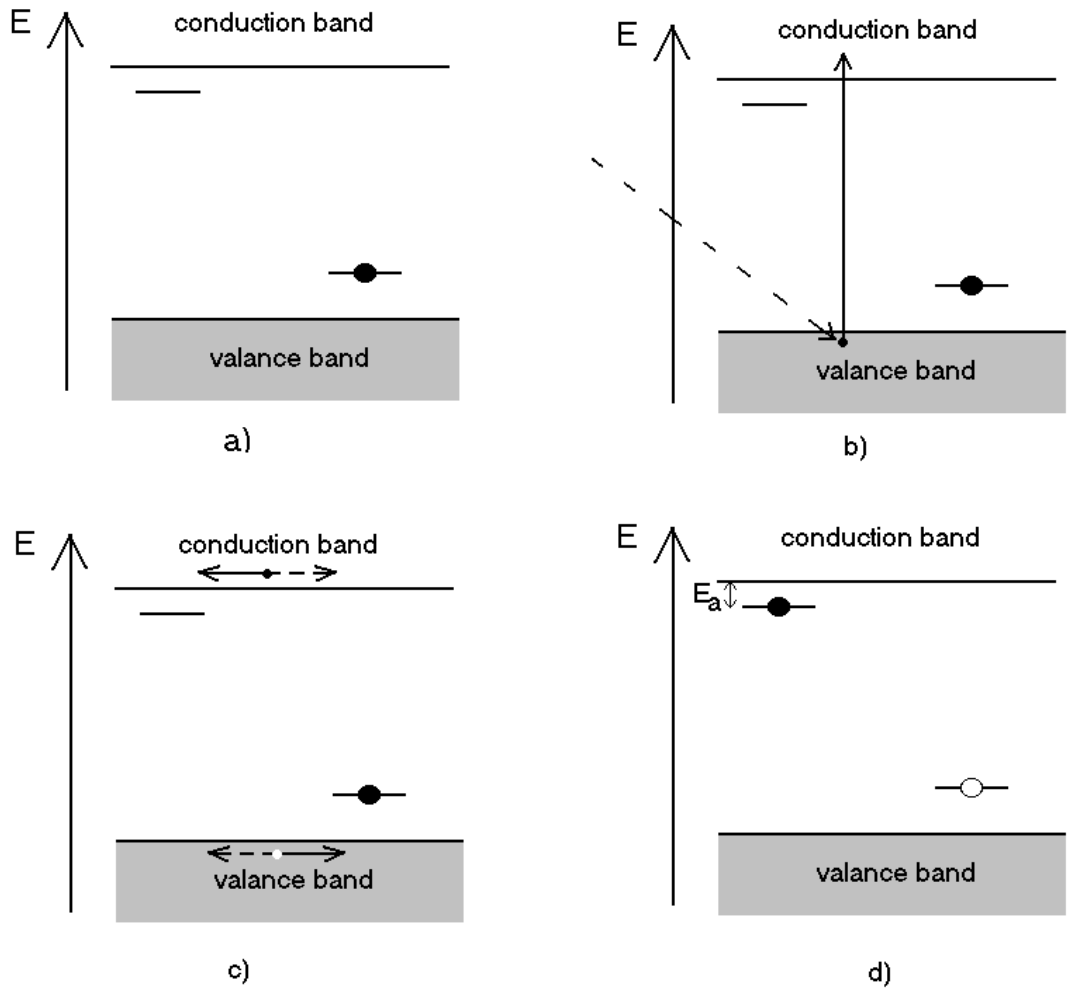

Figure 4.1: The simplified system of energy levels and the mechanism of trapping electrons in traps; a) the energy levels in the equilibrium state; b) ionising radiation has given an electron in the valence band enough energy to jump to the conduction band; c) a hole has been created in the valance band, while the free electron has jumped to the conduction band. Electrons in the conduction band and holes in the valence band may diffuse freely through the crystal lattice; d) final state – the electron has been trapped in the trap and the hole in the recombination centre.

The excitation energy needed to elevate an electron to the conduction band may be provided by light (photons) or heating (thermal energy). Some of the excitation energy is released as light (luminescence) if the electron recombines at a 'radiative' recombination centre; the rest is released as heat, if the electron recombines at a 'non-radiative' recombination centre. In case of external stimulation by heating, this phenomenon is called *thermoluminescence* (TL), in case of stimulation by light, *optically stimulated luminescence* (OSL).

The luminescence process has found application in archaeology and geology to date fluvial deposits, ancient pottery, lunar materials and other light exposed or heated materials. The lightsum emitted by the crystal lattice is proportional to the number of trapped electrons, and these in turn are dependent on the length of time a particular sample has been exposed to the natural radiation environment.

Optically stimulated luminescence is produced by exposing the crystal to light. The stimulating light should have an appropriately selected wavelength, because one must be able to distinguish the OSL signal to be measured from the light used to stimulate the material. The photon energy of the stimulating light must also be less than the energy needed to lift an electron from the valence band into the conduction band, otherwise fluorescence will mask the OSL signal lightsum. On the other hand, the energy of the photons in the stimulation light must be sufficient to excite the trapped electrons into the conduction band [Bluszcz, 2000].

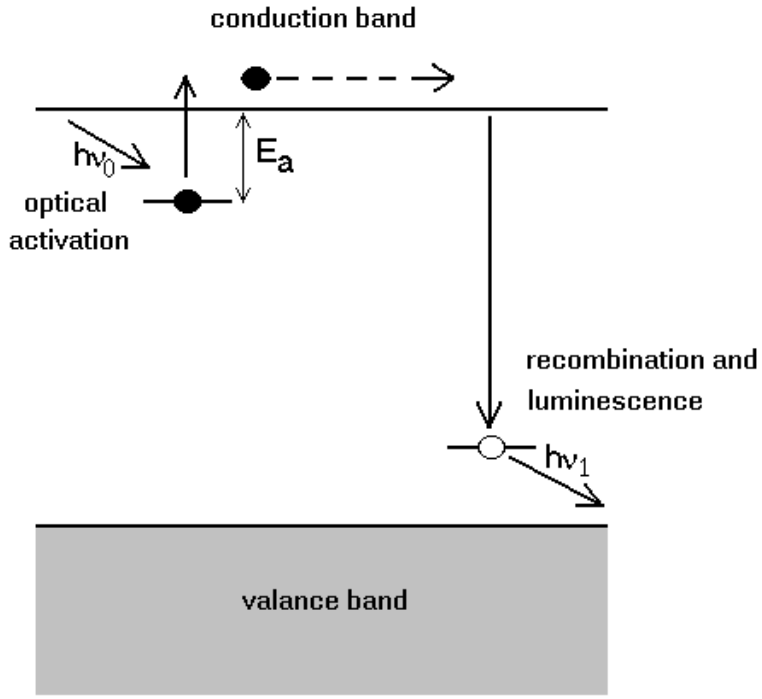

Figure 4.2: The luminescence process during light stimulation.

The intensity of a luminescence signal is not constant during stimulation with a constant power source; rather, the detected signal decreases approximately exponentially

with the time of stimulation. This behaviour is sometimes called the luminescence "shine-down curve".

4.2 The Single Aliquot Regenerative dose protocol

If the Single Aliquot method is used to measure the equivalent dose, D_e, only one aliquot is needed to make one estimate of the D_e; in the present measurements the single-aliquot regenerative-dose (SAR) protocol [Murray, 2000] was used. The SAR protocol consists of a repeated sequence of treatments as shown below:

Step	*Treatment*	*Measured signal*
1.	Give a regeneration dose, D_i[a)]	
2.	Pre-heat at temperature 260°C for 10 s	
3.	Stimulation for 40 s at 125°C	L_i
4.	Give a test dose, D_t	
5.	Heat to 160°C for 0 s (cut-heat)	
6.	Stimulation for 40 s at 125°C	T_i
7.	Return to step 1	

Table 2: Single-aliquot regenerative-dose (SAR) sequence.
[a)] for the natural sample when $i = 0$, $D_i = 0$.

The first OSL signal measured using the normal sequence of the SAR protocol (in step 3) is the natural signal, since initially no regeneration dose is given, $D_0 = 0$. The sample is preheated at step 2, and the natural signal measured by stimulation with blue light with a wavelength of 470(30) nm [Bøtter-Jensen, 2000]. Since only one aliquot is measured, the preheating step is very important when using the SAR protocol, as preheating removes all the "unstable" traps. For a sample taken from the natural environment (where it has been 'stored' for a long time) the problem of unstable traps is probably not very significant. It is when measuring the quartz directly after irradiation that the problem arises, because shallow light-sensitive traps can contain charge at the end of this process. If the quartz was not preheated immediately before being measured, then the apparent dose could be underestimated.

After stimulation of the natural signal, the sample is irradiated with a test dose, which is kept constant throughout the whole measurement sequence; the sample is then heated again, but only to a low temperature, to minimise sensitivity changes compared to the natural measurement conditions. The lightsum after applying the test dose and heating is measured in step 6. The test dose is repeated after each irradiation of the regeneration dose to check the sensitivity of samples is not changed during the sequence.

The regenerative sequence, in which D_i is given ('i' not equal to 0) is then undertaken using the same aliquot; this cycle can in principle be repeated as many times as is necessary. Two specific measurements are made to check the SAR protocol is working properly: a measurement of recuperation (D_4 = 0 Gy) and of a repeat point ($D_5 = D_1$, used to give the recycling ratio).

The recuperation test point is measured after at least 3 regenerative measurement cycles have been complete To measure a recuperation test point, a zero regenerative dose (D_4 = 0 Gy) is used. This is done to confirm that the growth curve actually passes through the origin of the graph of corrected OSL against dose.

The recycling test point is obtained after re-measuring the first regeneration dose somewhere in the sequence (usually at the end, i.e. D_5). The sensitivity corrected result after D_5 should be indistinguishable from that following D_5. This demonstrates that the sensitivity correction is working, and so that the measurements used to derive D_e can be trusted lightsum. The recycling measurement indicates whether or not it is possible to re-measure an aliquot, and obtain the same result.

4.3 Testing of the Risø OSL Reader

To examine if the equipment used for the measurements is causing any systematic errors in the results due to scattering of stimulation light in the detector, a number of tests were performed. First, a series of background measurements were made without any light stimulation; then another series of measurements was made with the calibration light turned on. Each measurement was made at room temperature, with an empty turntable placed in the reader. The detected counts were expected to be Poisson distributed (or close to) in both cases.

The background measurements were taken without any light stimulation at an ambient temperature of about 25°C. A single measurement lasted about 2 seconds with 4000 measurements taken. The average value for this set of data and for the expected Poisson distribution was found to be 41.6 counts per second with an expected standard uncertainty of the mean of 4.5 counts per second for the Poisson distribution. The experimental value observed, however, was 9.0 counts per second, e.g. larger than the value expected for a Poisson distribution.

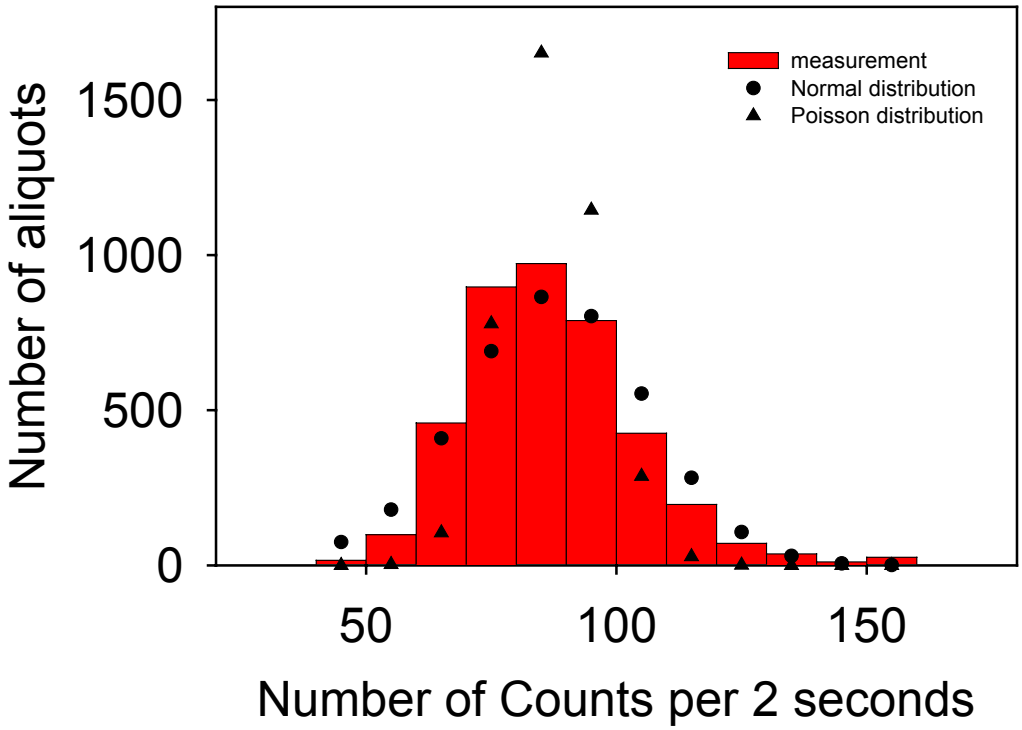

Figure 4.3: Histogram of counts detected at room temperature by the Risø OSL reader. The theoretical normal distribution indicated by the filled dots was based on the mean value of 41.6 and standard deviation 9.0 counts per second. The theoretical Poisson distribution indicated by the filled triangles was based on the mean value of 41.6 counts per second.

The results are shown in Figure 4.3. The theoretical normal distribution was calculated from a mean value of 41.6 and standard deviation 9.0 counts per second; the normal distribution is represented in the figure by filled dots. A χ^2 test was performed in

order to check the agreement between this distribution and the measured values. The test yielded $\chi^2_\nu = 81.22$ per degree of freedom, indicating a test probability close to zero.

The theoretical value of the Poisson distribution shown was calculated from the mean value of 41.6 counts per second. As it can also be seen from Figure 4.3 (values indicated by filled triangles) the agreement between the measured counts and the expected Poisson distribution is even worse than for the normal distribution; according to our expectations the histogram should have been much higher and narrower. This result was supported by performing a χ^2 test yielding a test value of $\chi^2_\nu = 8.4*10^8$ per degree of freedom. Thus, this experiment shows that the detected counts without any light stimulation do not follow the Poisson distribution.

Another set of measurements was made with the calibration light turned on at constant intensity. In order not to "blind" the PM tube due to the high number of counts, a blue filter was used during these measurements, reducing the number of photons reaching the detector to a suitable level. Otherwise, the experimental conditions were the same as before. Since the count rate was substantially higher each measurement lasted only 0.1 second. 2000 measurements were taken. During the measurements the count rate showed a tendency to decrease slightly, perhaps due to long term instability in the light source.

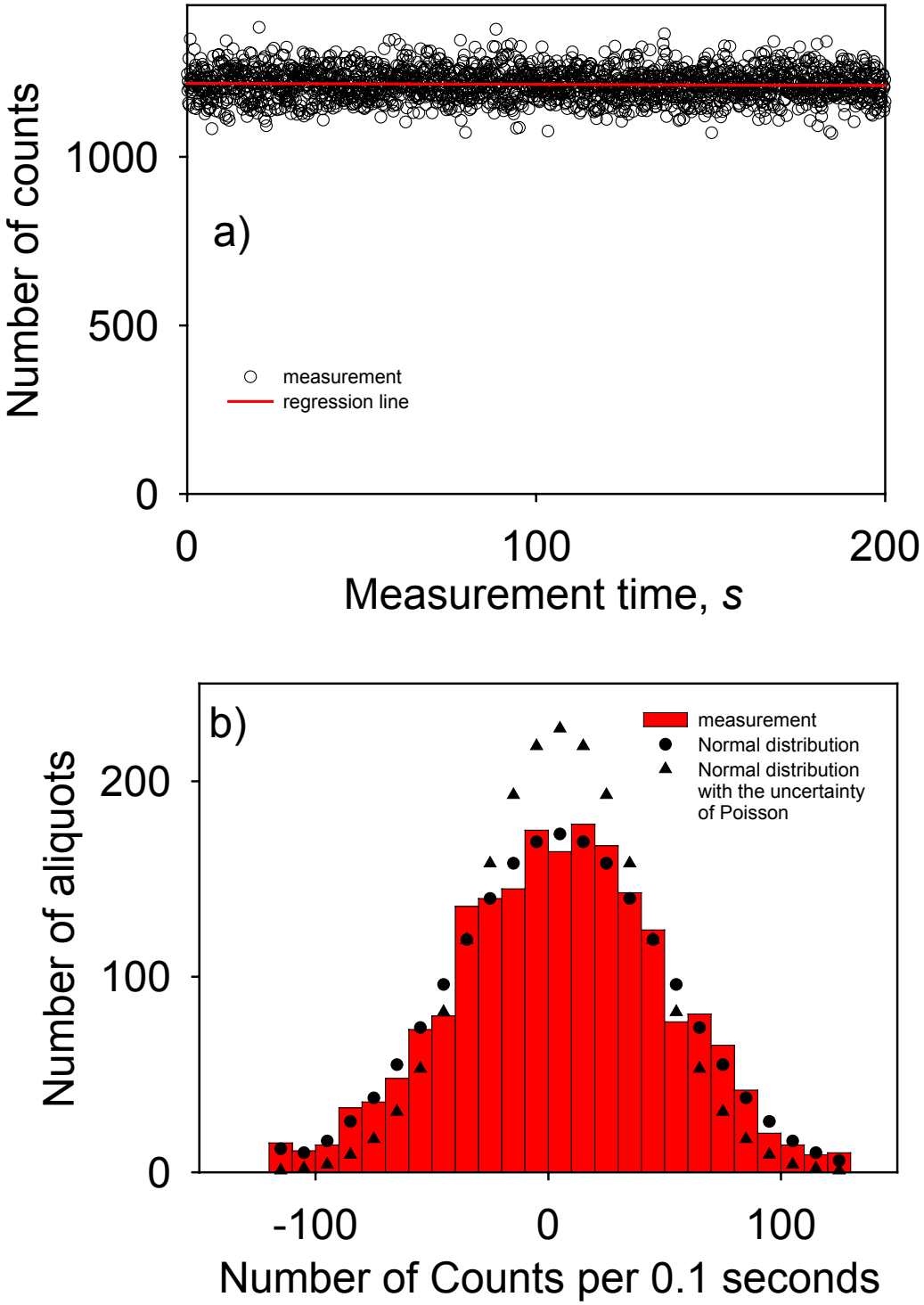

Figure 4.4: Counts detected at room temperature by the Risø OSL reader with the calibration light turned and a blue filter; a) the signal as function of measurement number (time) with the regression line; b) a histogram of the deviation of the observations from the regression line in (a) compared with a theoretical normal distribution based on the mean value of 0.0 and the standard deviation of 460 counts per second is indicated by filled dots. Another theoretical normal distribution with the standard deviation calculated as for a

Poisson distribution is indicated by filled triangles; this distribution has standard deviation of 350 counts per second.

Due to the tendency for the data to decrease with time, a straight line was fitted (y = -0.0031 * x + 1217.92, where y is the lightsum in x-th measurement) to the number of observed counts as a function of the number of measurements (Figure 4.4a), and the difference between the regression line and the measured values calculated. The distribution of differences is shown in Figure 4.4b, the theoretical normal distributions being calculated for different standard deviations. The distribution represented by filled dots was calculated using the standard deviation from the data set, while the distribution represented by filled triangles was calculated using the square root of the average value of counts (i.e. as in a Poisson distribution). In the first case, the standard deviation value used was 450 per second. Comparing this distribution to the data, a χ^2 test found $\chi^2_\nu = 0.99055$ per degree of freedom, yielding a probability of 47%. The data thus shows a very good agreement with this normal distribution. For comparison, a second distribution was calculated basing on the standard deviation of 350 per second. In this case, however, the χ^2 test fails, yielding a value of about 30 and a test probability close to zero.

Both experiments show that the actual scatter of results is significantly greater than expected for Poisson distribution. Additionally, at very low counting rates (cf., background measurements) the scatter is also not normal. At the higher counting rates, typical for OSL measurements, number of counts follow very well the normal distribution but with the standard deviation significantly larger than for the Poisson distribution with the same mean. All the physical processes involved should eventually lead to the Poisson distribution of number of photons counted during the measurements. Thus the greater scatter may be attributed to some additional non-Poisson processes in the reader, for example, fluctuations of excitation light power or fluctuations of a threshold level of the pulse discriminator, to mention just the most obvious possibilities. (The non-Poisson distribution of background counts hints at the second reason.)

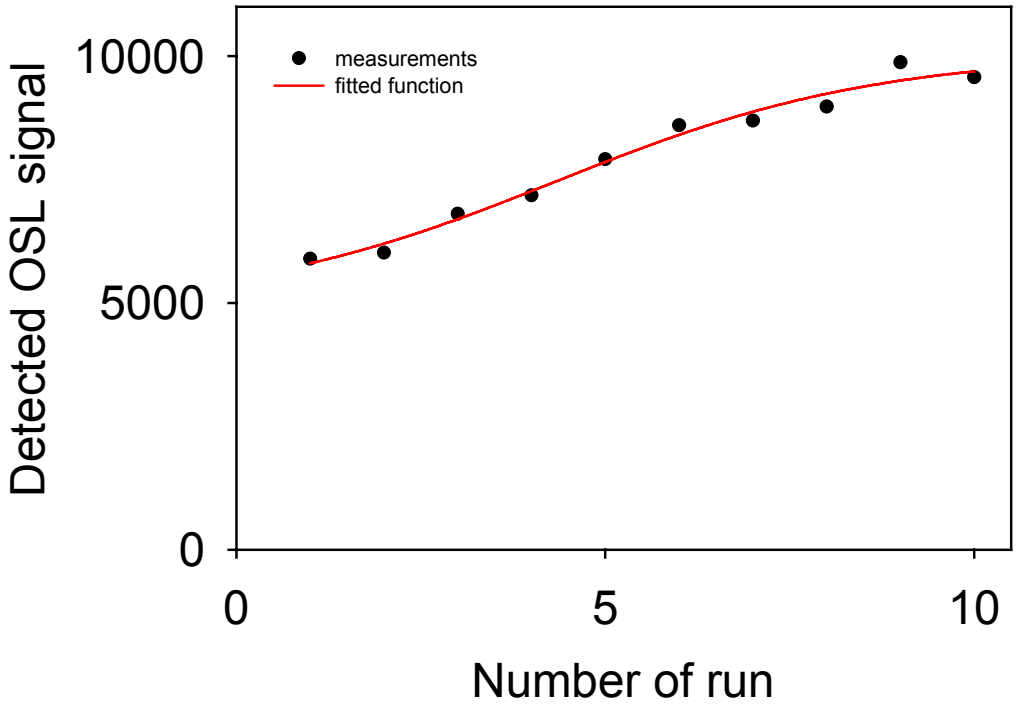

Figure 4.5: OSL measurements for a typical single aliquot of quartz with the best fit (disc no. 2). The *x*-axis is the number of irradiations using the same regeneration dose; the *y*-axis shows the lightsum in the first 0.8 second following each irradiation.

To estimate the overall instrumental error, another experiment was made. Prior to any irradiation or light stimulation, a quartz sample was optically bleached. The sample was then measured using the usual sequence of the SAR dose-response protocol (cf. section 4.2). During the experiment one regeneration dose was repeated 10 times. In the absence of sensitivity changes, the detected signal should have the same lightsum following each irradiation with the same regeneration dose. In fact, sensitivity changes do occur, but these vary smoothly with repeated dose. The lightsum was plotted as a function of the run number and a smooth curve fitted to through these points; this curve is used to represent the effects of sensitivity change through the experiment. For each point, the observed uncertainty was calculated as

$$\Delta_i = \frac{y_i}{y_i^{reg}} - \overline{\left(\frac{y}{y^{reg}}\right)}$$

These values include all sources of random uncertainty in the measurement of an OSL signal, i.e. instrument reproducibility in irradiation, sample positioning etc. and uncertainties arising from photon counting. The expected relative uncertainty of the detected signal was calculated assuming a Poisson distribution, and the square of these two values subtracted (cf. Table 3). The weighted mean of 10 discs yielding an uncertainty of 1.17(14)% (cf. Table 4). This value must in general be added to the uncertainty of the lightsum.

Number of run	y_i	y^{reg}	$\sqrt{\left(\frac{y_i}{y_i^{reg}} - \overline{\left(\frac{y}{y^{reg}}\right)}\right)^2 - \left(\frac{\sqrt{y_i}}{y_i}\right)^2}$
1	5894	5802	0.89%
2	6017	6199	2.62%
3	6804	6695	1.06%
4	7176	7263	0%
5	7909	7852	0%
6	8598	8403	2.05%
7	8691	8870	1.70%
8	8976	9235	2.60%
9	9874	9503	3.77%
10	9572	9689	0.63%
Average			1.53(39)%

Table 3: Example calculations for the example disc (disc no. 2) shown in Figure 4.5.

Number of disc	*Mean non-Poisson deviation*	*Uncertainty of the mean*
1	2.10%	0.44%
2	1.53%	0.39%
3	0.96%	0.52%
4	3.51%	0.85%
5	4.52%	1.07%
6	0.38%	0.25%
7	1.15%	0.55%
8	1.91%	0.83%
9	2.44%	0.73%
10	0.87%	0.31%
weighted average	**1.17(14)%**	

Table 4: Mean non-Poisson deviations (instrumental errors) for each disc.

4.4 Luminescence characteristics

To examine the behaviour of the quartz extracted from the Öggestorp samples, preliminary investigations of some relevant properties were undertaken; these included measurement of the growth curve, thermal transfer properties and a dose recovery test. Based on these tests the optimum conditions for the OSL measurements were chosen. In these studies almost all tests were made using the sediment from inside the stone structure, except for the thermal transfer test which was also made using a modern analogue sample – the topsoil.

4.4.1 Growth curve

The amount of light (lightsum) emitted by a quartz crystal is proportional to the number of electrons bound in traps in the crystal lattice. During a bleaching event all electrons bound in the lattice traps are unbound. If the quartz in the natural environment is subsequently "buried", some of the electrons are excited by the natural background radiation flux; these electrons then diffuse around the crystal lattice, where some of them will eventually become trapped in the lattice traps. Since the number of traps is finite, however, only some of these electrons are in fact trapped over time. The number of "free" traps decreases, and eventually all the traps are filled. This is called a saturation process.

To determine the shape of the growth curve for these samples, a typical SAR dose-response was measured. To derive the growth curve shown on Figure 4.6, a number of increasing regeneration doses were given sequentially. To probe the region of the expected apparent dose, D_e, the increase in dose for each step was initially small. The recycling point test was also measured twice to check that the measured quartz grains could be safely re-measured even after large regeneration doses. Each aliquot measured contained about 80 grains of cleaned quartz from sediment inside a stone structure, a clearance cairn (010411). The results, illustrated in Figure 4.6, are adequately represented by a single saturating exponential (see the fitted line). Initially, samples were measured using the normal sequence of the SAR protocol (three regeneration doses and a recycling point test; cf. section 4.2). Afterwards, extra regeneration doses were added to check the saturation conditions of the sample in the laboratory; usually the last regeneration dose is 10 times bigger than the average natural dose (here about 5 Gy). Finally, a recuperation and a recycling point tests were measured after the last regeneration dose.

The plots in Figure 4.6 show the measured recycling point tests as open triangles. The points shown were measured twice, one after three regeneration doses (after the 10 Gy point) and again after the last regeneration dose, in this case 50 Gy. The recycling test point was measured using the first regeneration dose after reading the natural signal. In this example the first regeneration dose is 2 Gy and the other 15 Gy. The average values for the recycling point tests for the three aliquots shown in Figure 4.6 are 1.032(14) and 1.013(28) for a regeneration dose of 2 Gy and 15 Gy, respectively. These recycling point tests of close to unity confirm that the same point may be measured repeatedly, confirming the reliability of the measured growth curve by OSL.

The dashed line shows how the apparent equivalent dose (D_e) for this aliquot may be interpolated using the dose-response plot and the natural OSL signal. The average value of three estimates of D_e, using three individual aliquots, is 7.137(80) Gy. The usual regenerative doses in the SAR sequence are between 3 and 13 Gy.

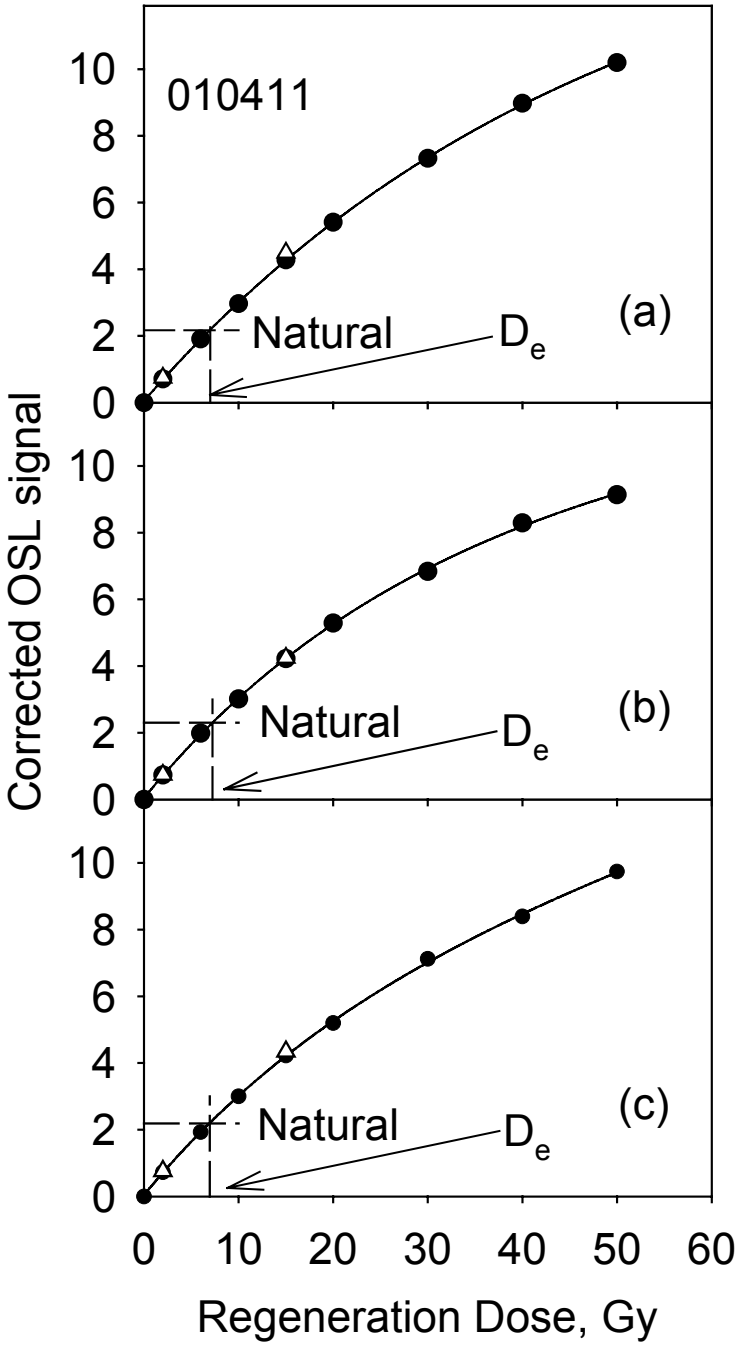

Figure 4.6: The growth curve for three aliquots (a,b,c) of sample 010411; filled circles – corrected OSL signal following various regeneration doses (R_i=L_i/T_i); dashed line – level of natural corrected signal (L_0/T_0) showing interpolation onto the growth curve to obtain the apparent equivalent dose, D_e; open triangles – the recycling points at 2 and 15 Gy.

4.4.2 Thermal transfer

When working with young material, one needs to check the recuperation processes of the sample in order to choose appropriate preheat conditions. Otherwise, these effects can have strong influence on the measured equivalent doses, as the preheating step of the dating sequence may introduce unwanted charge transfer. One such process is the *thermal transfer* [Aitken, 1998], which is a process of retrapping electrons.

In the SAR sequence (cf. section 4.2) a preheating step takes place following each irradiation (natural or regeneration dose); this step may have the unwanted effect of increasing the observed level of the subsequent OSL signal. In fact the preheating may increase the observed OSL signal so that it appears as if the sample had been irradiated with an *additional* dose (even if no dose had been administered) causing the subsequent measurement of the OSL to yield an overestimate of the equivalent D_e! This spurious OSL signal is thought to be due to the trapping of thermally excited electrons induced by the external heating [Aitken, 1998].

To help setting the correct preheat conditions the thermal transfer characteristics of three samples were examined, two infill samples (wall sample 010407 and clearance cairn 010411) and one modern analogue (modern topsoil sample 020401). For each sample, 24 aliquots were bleached at room temperature. Afterwards, the normal SAR sequence was started and the apparent equivalent dose measured as a function of preheat temperature from 160^{o}C to 300^{o}C. Figure 4.7 shows the results for the three selected samples, each point being the average of three aliquots (these aliquots were measured with the same preheat condition). For the modern topsoil, D_e increases from 0.00179(77) Gy at 160°C to 0.0060(32) Gy at 300°C. These values are small compared to the average value of the apparent dose (0.82 Gy). The apparent dose also increases for the two infill (010407, 010411) samples, from 0.0041(55) Gy at 160°C to 0.073(24) Gy at 300°C and from 0.0155(55) Gy at 160°C to 0.0406(55) Gy at 300°C, respectively. From these results the thermal effects found are clearly small, leading to the conclusion that this material is not significantly influenced by thermal transfer processes during the OSL measurement protocol. Hence, a preheat temperature of 260°C was chosen for the remainder of the measurements.

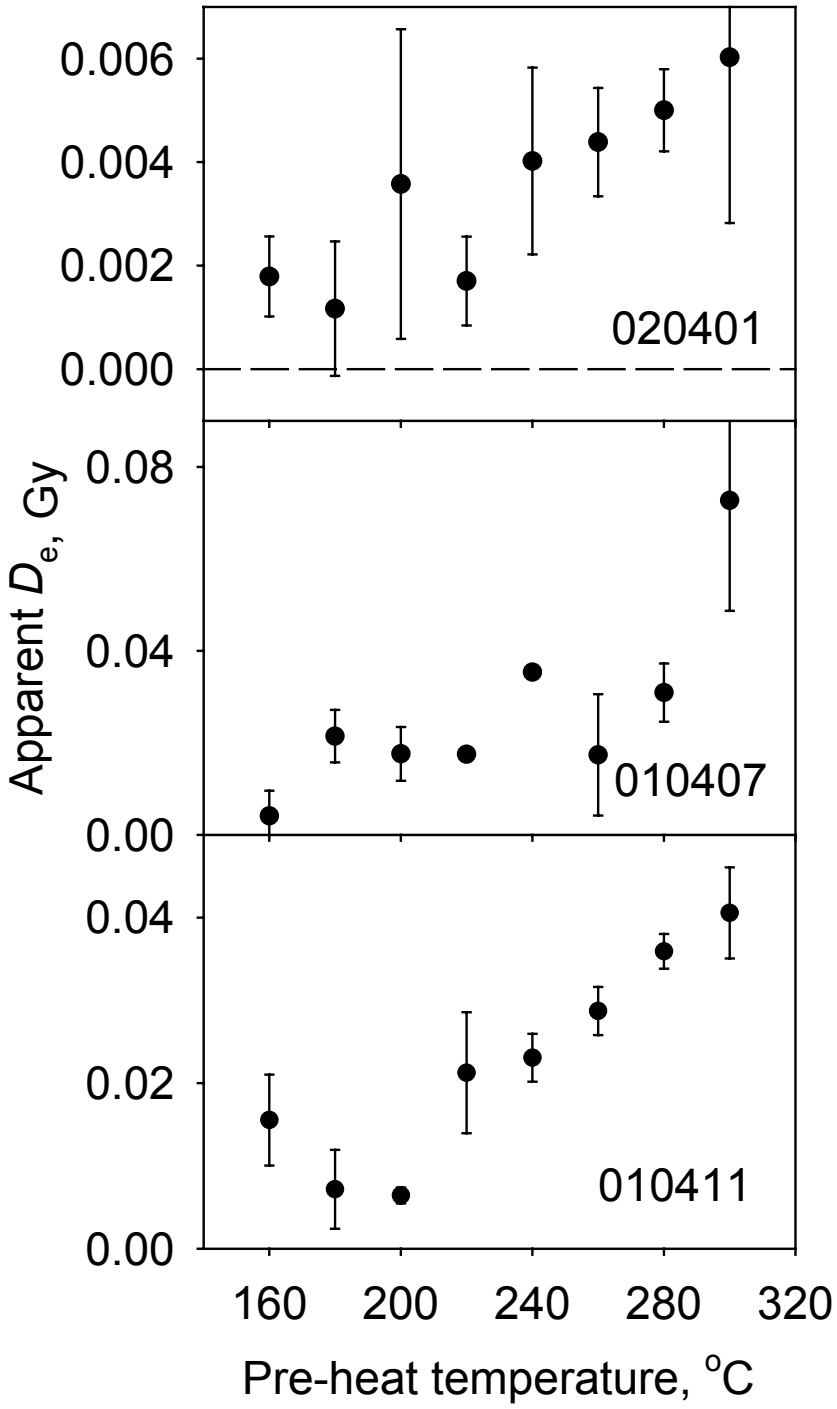

Figure 4.7: Thermal transfer for three different samples. The top figure uses the modern topsoil sample 020401, while the two bottom figures are from infill samples 010407 and 010411.

4.4.3 Dose recovery test

To check that no unwanted effects (e.g. arising because of the first heat treatment, or because of elevated temperature stimulation) take place during the measurement of the natural signal a dose recovery test was undertaken. For this purpose 48 aliquots that were initially light bleached at room temperature were studied. Subsequently, this unheated material was irradiated with a known beta dose of 7 Gy in the laboratory. The dose was then measured using SAR as a function of preheat temperature from 160°C to 300°C; the results are shown in Figure 4.8. The dose recovery test was made on material from sediment taken from inside a clearance cairn (010411).

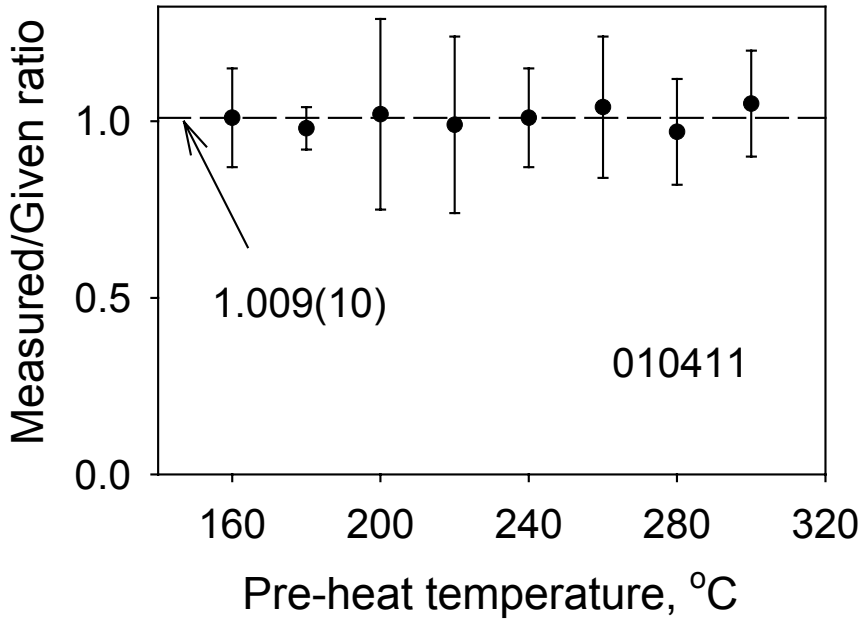

Figure 4.8: The dose recovery test. The figure shows the ratio of the apparent equivalent dose, D_e, measured as a function of preheat temperature to the known dose given in the laboratory, after illuminating the aliquots with light at room temperature. 48 aliquots were measured.

Each point represents the average of 6 aliquots. The average value of measured/given ratio over the entire temperature range from 160°C to 300°C is 1.009(10) (the number of aliquots is 48). From the results found it was concluded that no unwanted effects are present in the experiment. Thus a known laboratory dose given to the sample before any thermal treatment may be measured exactly.

4.4.4 Dependence of bleaching on grain size

To examine the degree of bleaching of the quartz grains as a function of their size, three different samples from sediment inside stone structures were investigated (010402, 010404 and 010411).

During the initial sieving of the samples, the quartz grains were divided into groups based on their size. The largest number of grains lay in the size range 90-180 μm. The size-sorted grains were then chemically cleaned (cf. Appendix A). This reduced the number of grains substantially, indicating a significant amount of carbonate and feldspar, especially in the larger grain size fraction. Additional problems were found with the largest size fraction (500-1000 μm) particularly for samples 010402 and 010411 where the contamination by feldspar (as detected by infrared stimulation) was found to be unusually high. These samples were eventually treated with concentrated HF three times each treatment lasting one hour. After each reaction, the samples were sieved again keeping only those grains larger than 500 μm; as a result of the HF treatment, many of the bigger grains simply fell apart, indicating that the grains were formed of a mix of feldspar and quartz. After the acid treatment, the remaining feldspar contamination was assessed issuing infrared stimulation.

A series of measurements was undertaken using sample 010404, using groups of aliquots, each group with a different number of 180-250 μm grains per aliquot. Initial measurements were made using about 120 grains arranged in the middle of an aluminium disc within a circle of 3 mm diameter. This was done achieved using an appropriate spray mask to coat the middle of each disc with thin silicone layer to retain the grains during measurement. 48 aliquots of chemically cleaned quartz grains were used in these initial measurements, and the observed equivalent doses are shown on Figure 4.9 (upper part). The histogram is approximately symmetric with a mean value of 8.10(37) Gy. Because an aliquot contains about 120 grains, the result from each aliquot already represents an average D_e, thus obscuring the true dose distribution. From a consideration of the approximate dose rate within this stone structure (see Chapter 7), one might expect to find at least a few grains with doses between 0 and 5 Gy. This is because, after construction of a wall or cairn, wind and rain are likely to have deposited at least some grains in the structure after construction. Any such details, however, are lost due to the averaging of doses because of the number of grains present in the 3 mm sample. This sensitivity to averaging is a problem for any Single Aliquot method, if the sample is suspected of being

partially bleached. In practice, for any sample one must seek a compromise between the amount of light emitted by an aliquot lightsum and the degree of dose averaging. This is clearly also a function of the fraction of grains emitting light [Duller and Murray, 2000; Duller *et al.* 2000].

Consequently, the distribution of apparent doses for aliquots with a diameter of 2 mm was also examined; in this case about 80 grains are mounted on each disc. Results of measurements using such aliquots are shown on the lower part of Figure 4.9. The histogram includes results from 192 aliquots. In this case one does observe a few aliquots with apparent doses in the range from 0 to 6 Gy. One also observes some aliquots with much larger apparent doses than before; overall the total range is wider than for the 3 mm aliquots. This histogram is also asymmetric, and reveals important structure in the dose distribution – especially in the lower dose region. Nevertheless, using the Single Aliquot method (even with 2 mm aliquots) some averaging must take place; using smaller aliquots one is able to decrease the degree of averaging, but the only way to remove this effect completely is to measure the equivalent doses from individual grains.

From a consideration of the averaging effect of larger aliquots and of the lightsum observed following the test doses (cf. Table 5), it was concluded that all single aliquot measurements should be performed on 2 mm aliquots, each containing about 80 grains. Using the sub-aliquot in the single aliquot method, it could be gotten results with very good precision. The overall lightsum from the sub-aliquot is dominated only by few grains.

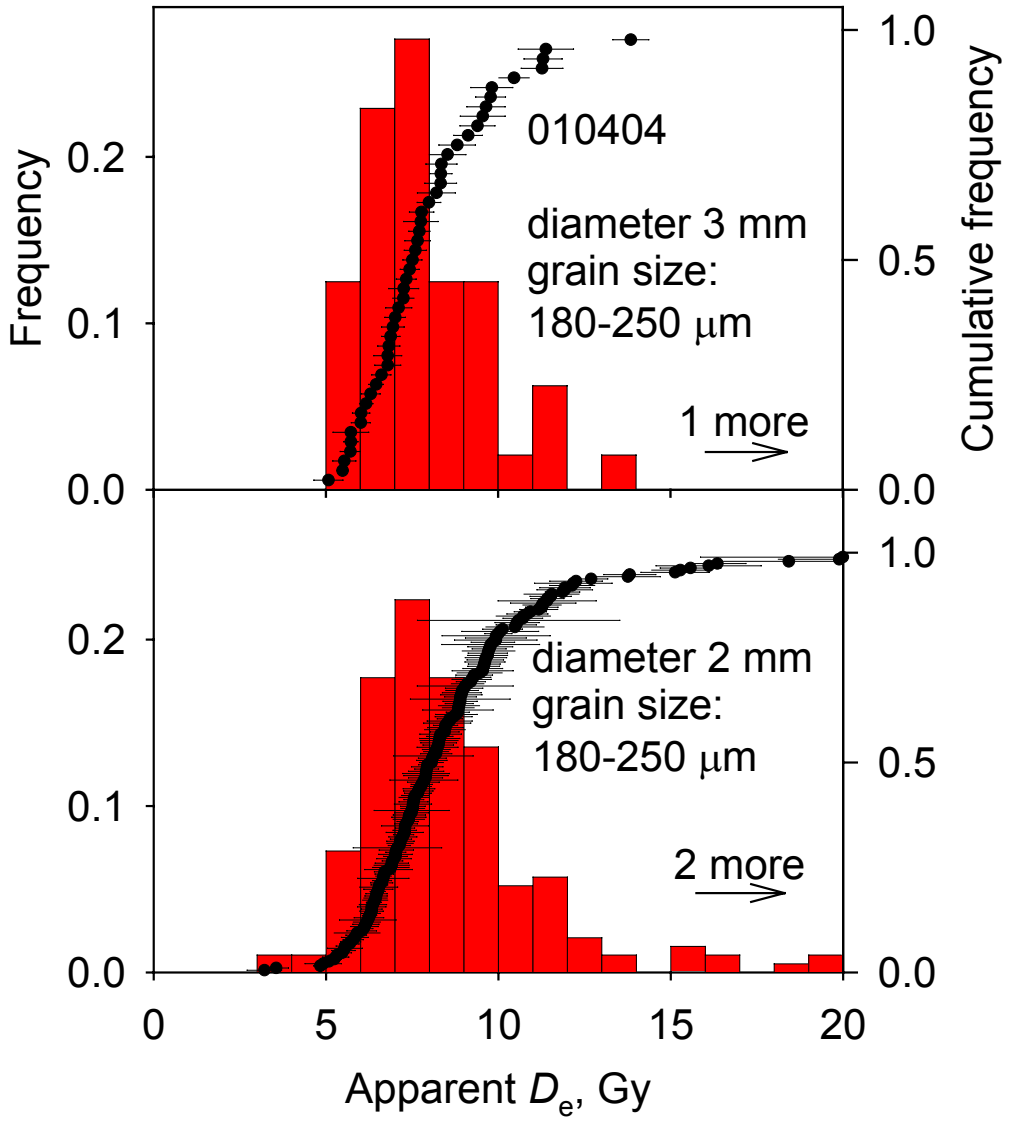

Figure 4.9: Histogram of doses observed using sample 010404 with a two different aliquot sizes; the upper plot represents a histogram using 3 mm diameter aliquots (about 120 grains; measured 48 aliquots), the bottom plot the results for 2 mm diameter aliquots (about 80 grains; measured 192 aliquots). The filled circles show the cumulative frequency as a function of apparent dose as well as the uncertainty of each measured dose using the Single Aliquot method. The *x*-axis is the apparent equivalent dose, the left *y*-axis the frequency of aliquots found for the given bin width, the right *y*-axis is the cumulative frequency. The frequency is defined as the number of aliquots divided by the total number of measured aliquots.

Each of the samples was assigned an appropriate test dose based on the aliquot sensitivity of the sample. In practice, most of the measured samples were given the same test dose (~2 Gy).

The measured lightsum for each grain sizes is shown in Table 5. To compare these results, one needs approximately the same number of grains in each aliquot. To check that the number of grains was indeed about 80 grains independent of grain-size, representative aliquots were prepared and the number of grains counted under the microscope. To put the same total number of grains on the discs, masks were used with different diameters (1 mm, 2 mm, 3 mm or 8 mm) depending on the grain sizes.

Grain size	*010402*		*010404*		*010411*	
	Average lightsum	*No. of aliquots*	*Average lightsum*	*No. of aliquots*	*Average lightsum*	*No. of aliquots*
90-180 μm	660(70)	96	920(100)	96	960(80)	96
180-250 μm	860(55)	192	2050(200)	48	530(60)	48
			1550(90)	192		
250-300 μm	2000(200)	96	4700(490)	96	3380(320)	96
300-500 μm	-	-	3530(600)	48	-	-
500-1000 μm	-	-	13700(1000)	96	-	-

Table 5: The net lightsum after a fixed test dose of approximately 2 Gy. The values given in the table corresponds to counts in the first 0.8 seconds (background subtracted); main column is for a different sample, and each row is for a different grain size. The lightsum was calculated using the sum of the contents of the first 5 measurements, each 0.16 s; the background was estimated by summing the last 25 measurements (4 s) and then deriving the average background over 0.8 s.

As shown in Table 5, the lightsum observed from each sample for a given grain size is different. When the lightsum of a sample is small, the sample is dim and the uncertainty on the apparent dose will be large. On the other hand, when measuring the apparent doses from bright samples, a greater precision can be expected. Naturally, one wants to make use

of only those samples with the smallest uncertainty when interpreting distributions of equivalent dose. Furthermore, Table 5 shows a dependence of the light intensity and the grain size, with larger grains giving more light. Presumably this is because larger grain aliquots have more mass.

Figure 4.10-13 shows histograms similar to Figure 4.9 for samples of different grain size but for approximately 80 grains per aliquot. The frequency distributions from one sample to another appear to be quite similar; there is no significant difference between the grains of different size. This suggests that grains from the same samples are bleached to the same degree regardless of size.

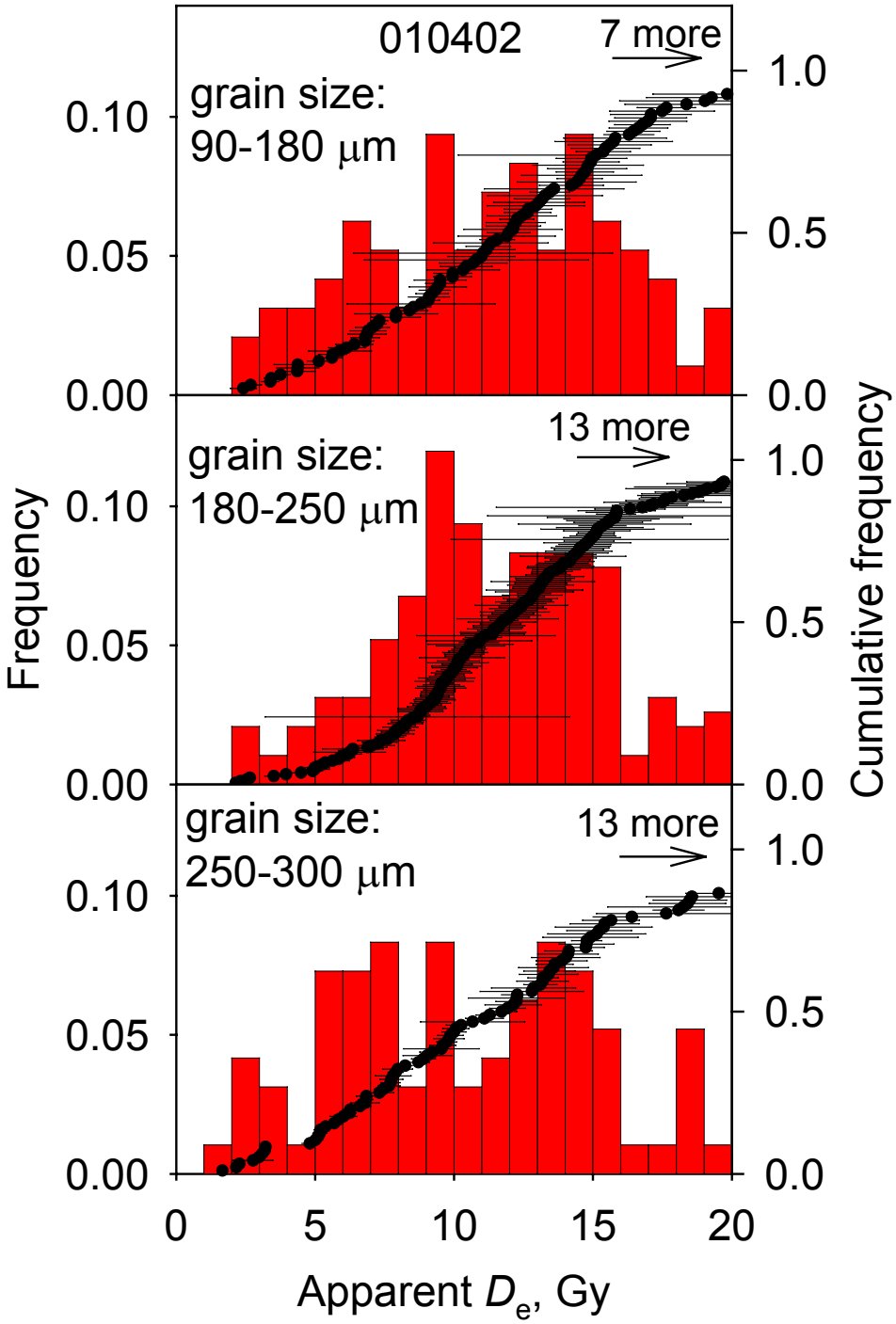

Figure 4.10: Dose distributions from sample 010402 for different grain sizes. The filled circles show the measured D_e value with uncertainty bars; these points form the cumulative frequency plot. The number of measured aliquots is 96 with the exception of grain size 180-250 μm where n = 192.

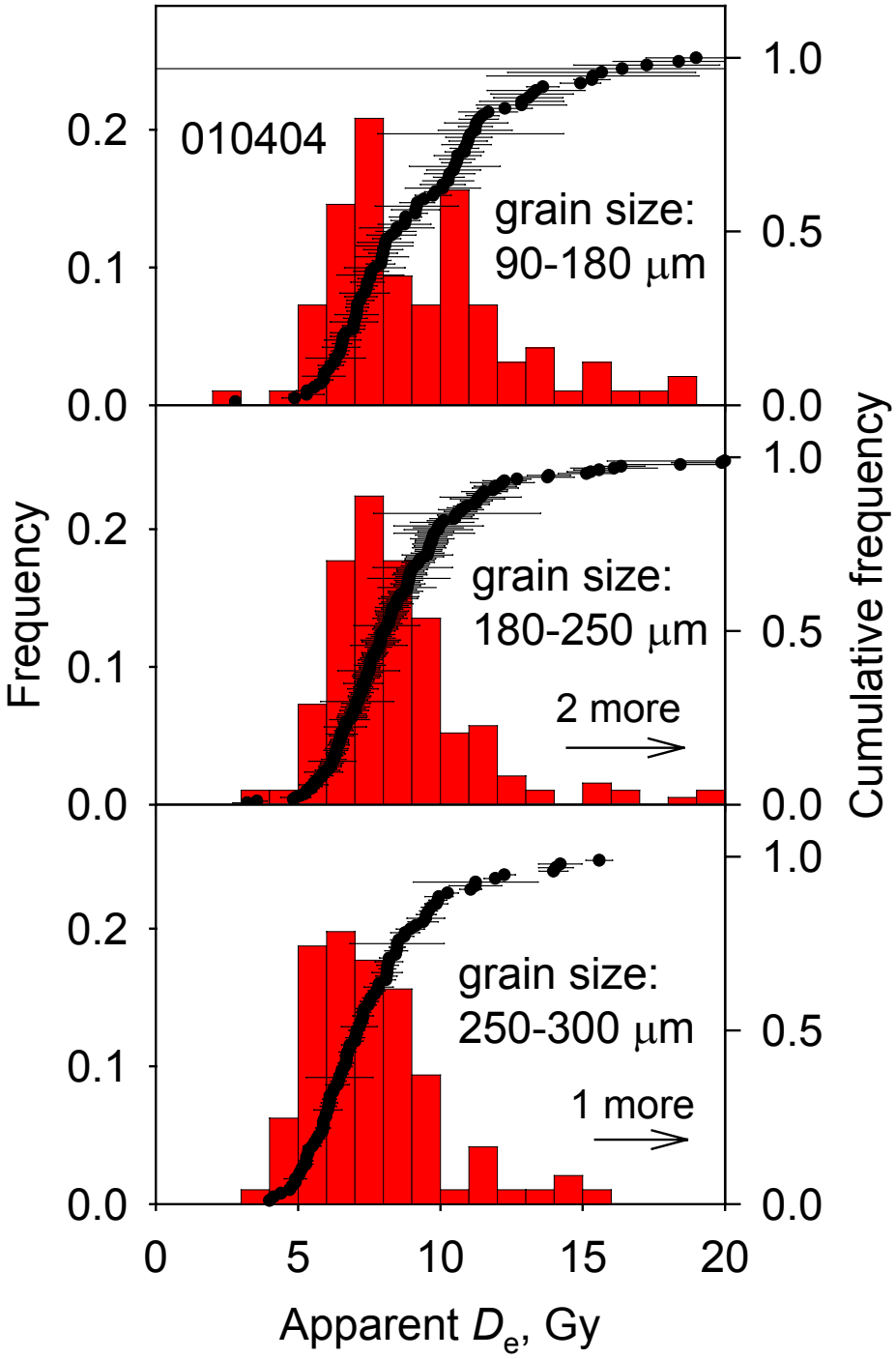

Figure 4.11: Dose distributions from sample 010404 for different grain sizes. The filled circles show the measured D_e value with uncertainty bars; these points form the cumulative frequency plot. The number of measured aliquots is 96, with the exception of grain size 180-250 μm where n = 192.

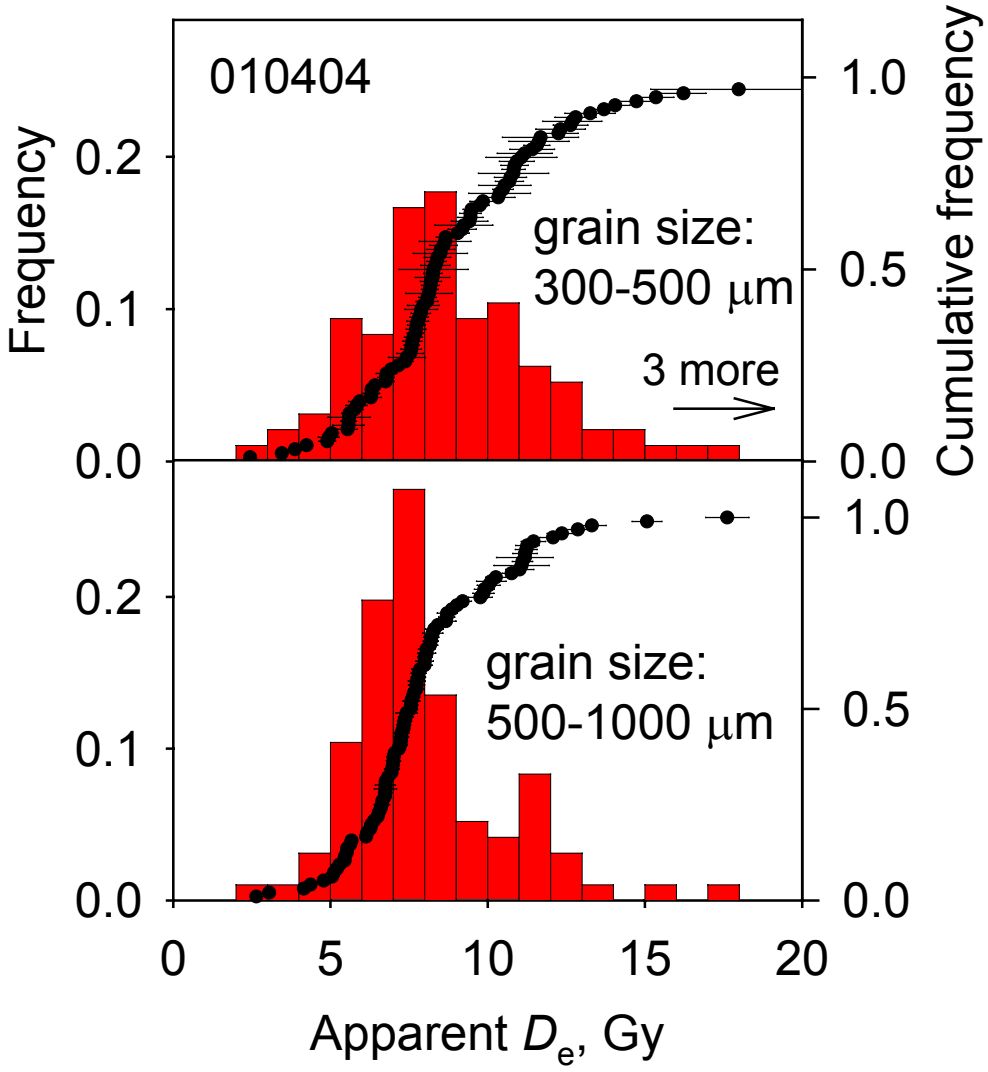

Figure 4.12: Dose distributions from sample 010404 for different grain sizes. The filled circles show the measured D_e value with uncertainty bars; these points form the cumulative frequency plot. The number of measured aliquots is 96.

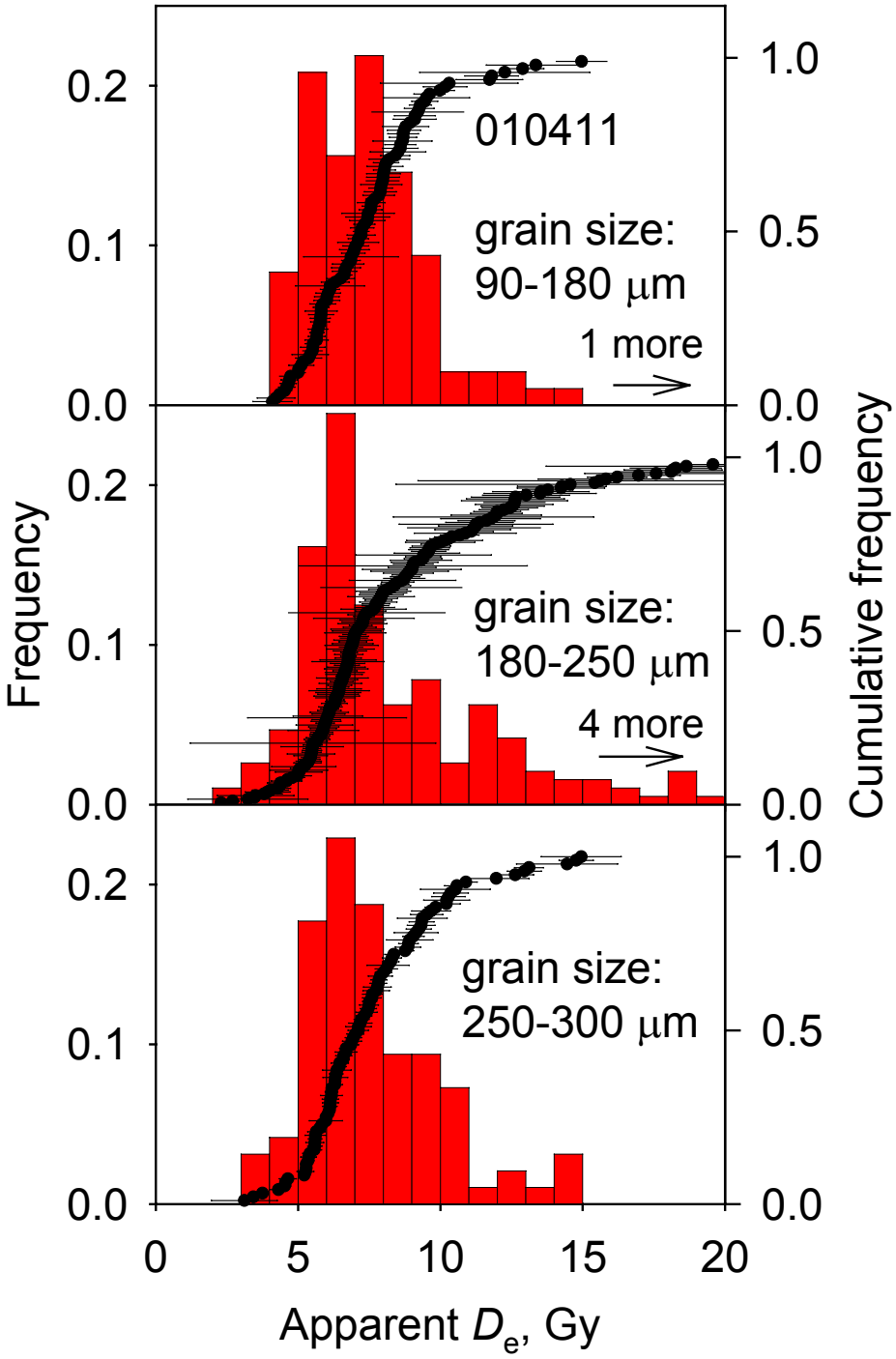

Figure 4.13: Dose distributions from sample 010411 for different grain sizes. The filled circles show the measured D_e value with uncertainty bars; these points form the cumulative frequency plot. The number of measured aliquots is 96 with the exception of grain size 180-250 μm where n = 192.

To summarize, several tests were performed in order to determine the right grain size to be used for the OSL measurements. The aspects considered for selecting suitable samples were the level of brightness, the degree of bleaching and the ability to select clean quartz grains of the right size. The size of the grains was found to have no significant influence on the degree of bleaching. The frequency of finding "clean" quartz grains apart from the technical aspects, however, clearly favoured the smaller grains as the larger grains were found to be more likely contaminated with feldspar. Considering the grain size between the 90-180 μm and 180-250 μm and the properties of brightness discussed above, the grain size of 180-250 μm was finally chosen for all subsequent single aliquot measurements.

4.5 Conclusion

To check the OSL reader, background counts detected by the photomultiplier tube at room temperature without any light stimulation were measured; the live time of each measurement was 2 seconds. The resulting distribution was compared to a theoretical Poisson distribution and found to disagree, the Poisson distribution being higher and narrower than the experimental one. An analogous result was found for a theoretical normal distribution. To examine this further, another test was made at room temperature with the calibration light turned on and a blue filter protecting the photomultiplier. Due to a tendency for the signal to decrease with time, a line was fitted through the observations; the measured values and the fitted points were then subtracted. The resulting difference distribution is centred on zero, and was compared to a normal distribution. Good agreement was found with the measured distribution, the probability of a χ^2 test being 47%. A similar normal distribution using the Poisson uncertainty as input, however, gave poor agreement. Contrary to expectations, the standard deviation and the square root of the average number of the counts were different for a large number of observations. This suggests some additional source of random errors. From measurements on optically bleached quartz samples with repeated applications of the regeneration dose, an overall instrumental uncertainty resulting from this source was estimated to be 1.17(14)%; this must be added to the uncertainty on the lightsum for all samples (Table 4).

The thermal transfer properties, the growth curve and a dose recovery test were then measured in order to determine suitable conditions for routine OSL measurements.

Measurements used to construct the growth curve for sediment-fill sample 010411 were found to behave well. It was assumed that all infill samples would behave in the same way. As is shown on Figure 4.6, the growth curve increases smoothly with increasing regeneration doses. Also, it was found that for doses between 0 and 13 Gy the growth is close to linear. This allows the use of only two regeneration doses, with linear interpolation of the corrected natural signal, without significantly increasing the uncertainty in dose estimation. Due to the likely age range of these samples, and the typical dose rates (see Chapter 7) one is only interested in equivalent doses in the range of 0 to 13 Gy.

The thermal transfer properties were measured for three different samples: a modern analogue (topsoil), an infill sample from the wall and sediment inside a clearance cairn. This kind of test is usually made on young material due to the possibility of increasing the apparent dose because of thermal transfer during preheating. The lowest thermal transfer was detected for the modern material and was less then 0.0060(32) Gy for preheating at 300°C; for infill material from the wall the equivalent value was 0.073(24) Gy at 300°C and for the clearance cairn 0.0406(55) Gy at 300°C. From this test it was concluded that these infill samples do not show significant thermal transfer at the preheat temperatures likely during routine measurements.

The dose recovery test was done to check that no unwanted alteration in the sample behaviour was triggered by the measurement process. After bleaching the samples, and prior to any preheating, samples were irradiated with a known dose; the aliquots were then heated to different temperatures in the range of 160°C to 300°C before reading the regeneration dose. An average value of measured/given ratio of 1.009(10) was found for 48 aliquots (sample 010411) covering the entire range of preheat temperatures. It was thus concluded that the samples showed no significant changes due to preheating. For routine measurements a preheat temperature of 260°C was selected.

A final series of measurements were performed in order to select the most appropriate grain size to use for routine measurements (using the preheat temperature found for the previous tests) as well as to select an appropriate number of grains to put on each disc. The first measurements were conducted with different numbers of grains of the

same size on the discs; it was observed that for the discs with a larger number of grains (~3 mm of diameter for the grain size 180-250 μm) the degree of averaging over the apparent doses was significant and thus the equivalent dose distribution rather symmetric. Looking at the dose distribution using smaller aliquots (~2 mm diameter, approximately 80 grains) the effect of averaging is clearly reduced; the histogram is more asymmetric and shows more structure. From these observations it was decided that further measurements should be made on discs with about 80 grains per disc (~2 mm for the grain size 180-250 μm). From measurements performed using different grain sizes but with approximately the same number of grains per aliquot, the lightsum after irradiation of the test dose was observed to be different from one grain size to another (Table 5). Additionally, after chemically cleaning the quartz, various fractions of the initial mass were left for each size, with the best recovery (highest fraction of quartz) coming from grains in the range 180-250 μm. From the distribution of equivalent doses with different grain sizes (cf. Figure 4.10-13) there was apparently no significant difference, all grain sizes were bleached to the same degree. Hence, since extracting the quartz from the largest grains was found to be more difficult than for the smaller grains, and from considerations of the sensitivity to the test dose (and of course the amount of clean sample recovered) grains in the size range 180-250 μm were selected for further measurements.

5 Dose distribution in unheated material

This chapter presents the results of measuring dose distributions from various samples taken inside and below the stone structures and also from above and below the hearth at the archaeological site at Öggestorp. All the samples discussed in this chapter were unheated before deposition and were measured using the Single Aliquot Regenerative dose method. For comparison, additional measurements were made on infill and aeolian (above the hearth) samples using the Single Grain Regenerative dose method.

5.1 Single Aliquot Regenerative dose method

In the following sections the sample measurements using the Single Aliquot Regenerative dose method will be discussed in detail.

5.1.1 Modern material from a demolished building and from topsoil

For reference purposes the dose distribution for two modern samples were measured, one from a building demolished during the last 10 years and the other from topsoil from within an adjacent wood. The sediment taken from between the bricks of a demolished building is assumed to be analogous to a sediment sample from between stones in a stone structure. It is assumed that the sediment between the bricks began to accumulate immediately after demolition, and the degree of bleaching reflects the natural light exposure of such material before being trapped in the building rubble. The purpose of these measurements is to examine the probable degree of bleaching in small aliquots of sediment infill samples.

The distribution of apparent dose for the modern infilling sediment sample (020402) is given in Figure 5.1. To study this sample, aliquots containing about 80 grains having sizes from 180 to 250 μm were used as described in the previous chapter. The sample is clearly incompletely bleached; the median of the distribution is about 1 Gy, and a statistical mean value of the distribution shown is 2.02(50) Gy. The distribution is markedly asymmetric [Wallinga, 2002], and there is a range of doses from close to zero up to more than 20 Gy. Nevertheless it appears that some aliquots do contain only grains that are well bleached (those with doses close to zero).

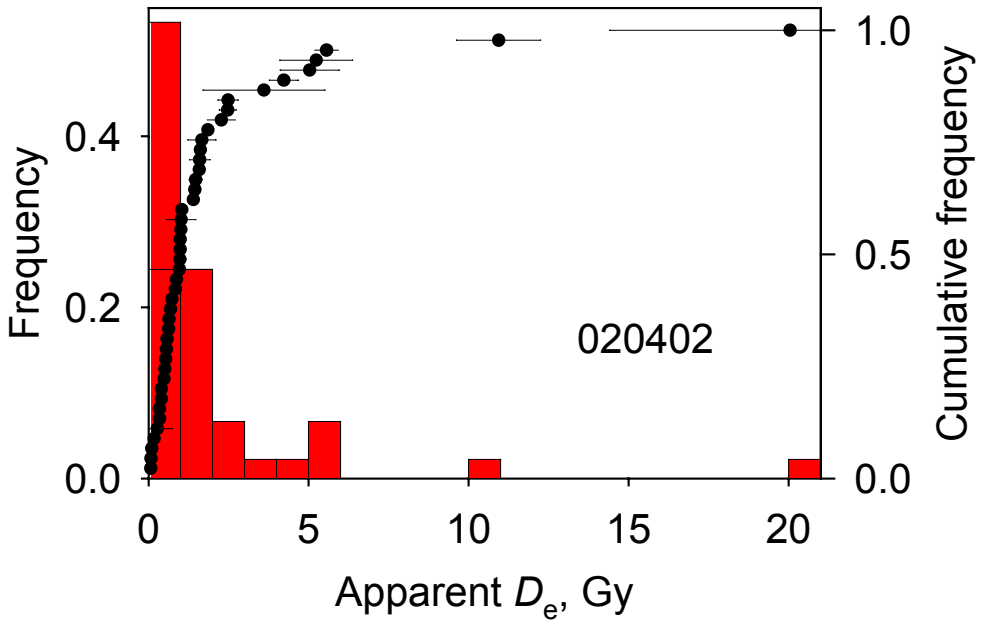

Figure 5.1: Histogram of equivalent doses, and cumulative frequency as a function of D_e, for sediment from between the bricks of a building destroyed in the last 10 years. The figure shows the results of measuring 48 aliquots.

The other modern material originates from topsoil taken close to the archaeological site to examine the degree of bleaching of the modern soil. It is presumed to be similar to that at the time the stone structures were built on the topsoil of the time. Surface soil mixing and light exposure will be heavily influenced by natural biological dynamics induced by the local flora and fauna as well as the weather. It is a system in constant motion. During the changes due to the bioturbation, soil grains are exposed to daylight, and so the accumulated dose is set to zero. Because of this, the luminescence system is continuously changing; one layer of soil grains is bleached and immediately local fauna, flora and wind or rain brings new grains to the surface, to cover the old layer, and form a new layer. Now each grain in the old, now light protected, layer begins to accumulate a dose. It is assumed that similar processes took place in the past, before the building of the stone structure, and that human activity did not remove the surface of the soil before building the wall or cairn. Hence, putting the stones on top of the soil surface effectively stops the natural process of zeroing the topsoil.

The measurements were performed using the Single Aliquot Regenerative dose method, each aliquot containing about 80 grains.

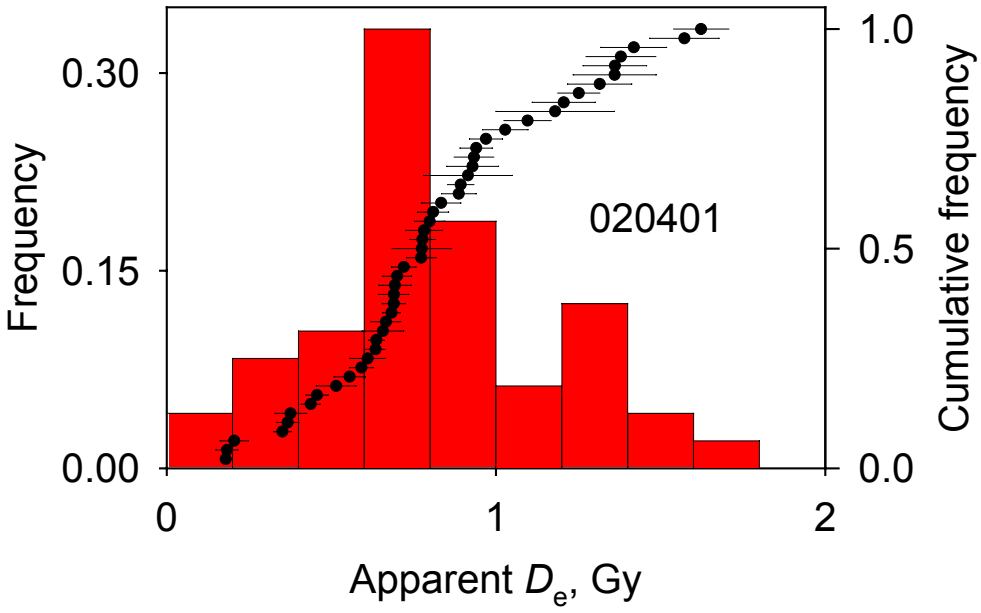

Figure 5.2: The histogram of values of D_e and the cumulative frequency as a function of D_e for the topsoil. The figure shows the results of measuring 48 aliquots.

The results for the sample from the modern topsoil (020401) are shown on Figure 5.2. The mean value is about 0.821(51) Gy. The apparent dose distribution is found to be symmetric, proving that this sample is either well bleached, or that the averaging within each aliquot is too great to reveal the true dose structure [Olley et al., 1999].

5.1.2 Aeolian sand above a hearth

Figure 5.3 shows the dose distribution from a sand sample taken just above the hearth (fireplace) (010414). The equivalent dose distribution is clearly symmetric and very narrow, so the mean value of 5.32(11) Gy describes the highest point of this distribution perfectly. The narrow distribution suggests that the sand was well bleached before deposition; this degree of bleaching is expected for aeolian sediments.

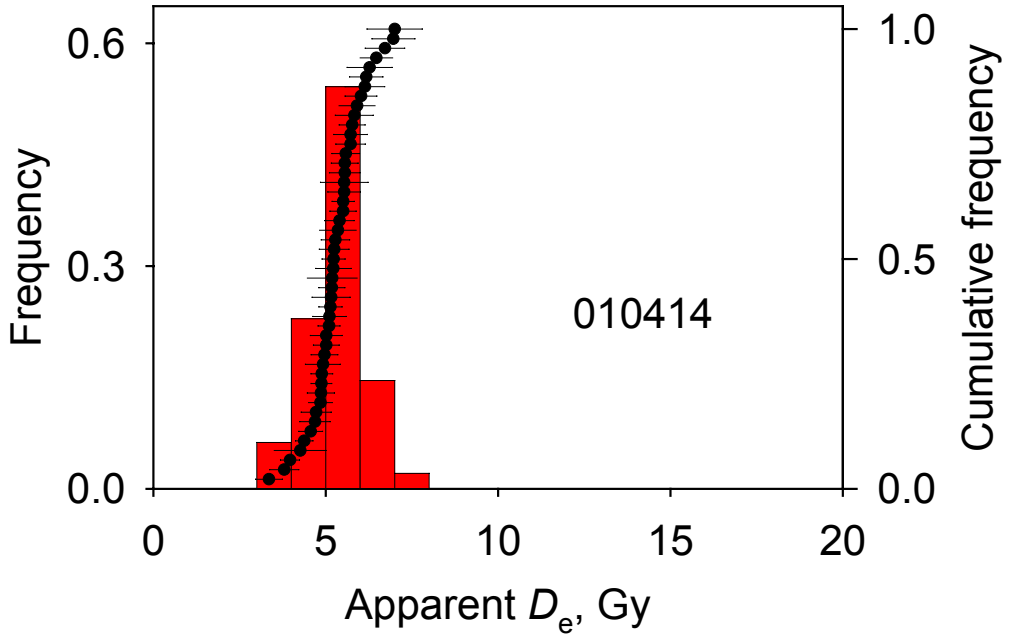

Figure 5.3: The distribution of D_e and the cumulative frequency as a function of D_e for the aeolian sample. The mean value is 5.32(11) Gy. The figure shows the results of measuring 48 aliquots.

5.1.3 Sediment from inside stone structures

It is assumed that during the building of the stone structures at Öggestorp, the stones used were not cleaned of any attached soil. During later periods, wind and rain will also add new grains to the structure; as a result sediment collected through time may be found between the stones in such a structure. Samples were taken from these kinds of sediments. The places of sampling are shown on Figure 3.1, the numbers 02, 04, 07, 09 indicating samples taken from different places of the wall, while the number 11 indicates a sample taken from a clearance cairn. A clearance cairn is a pile of stones from the nearest surroundings. It was created to clean a nearby field, usually for human activity such as non-agricultural use. Its location was often a corner of field, and a compromise between finding an unused place and distance.

Figures 5.4-5.8 shows the results for the five samples listed above, taken from inside the wall and clearance cairn.

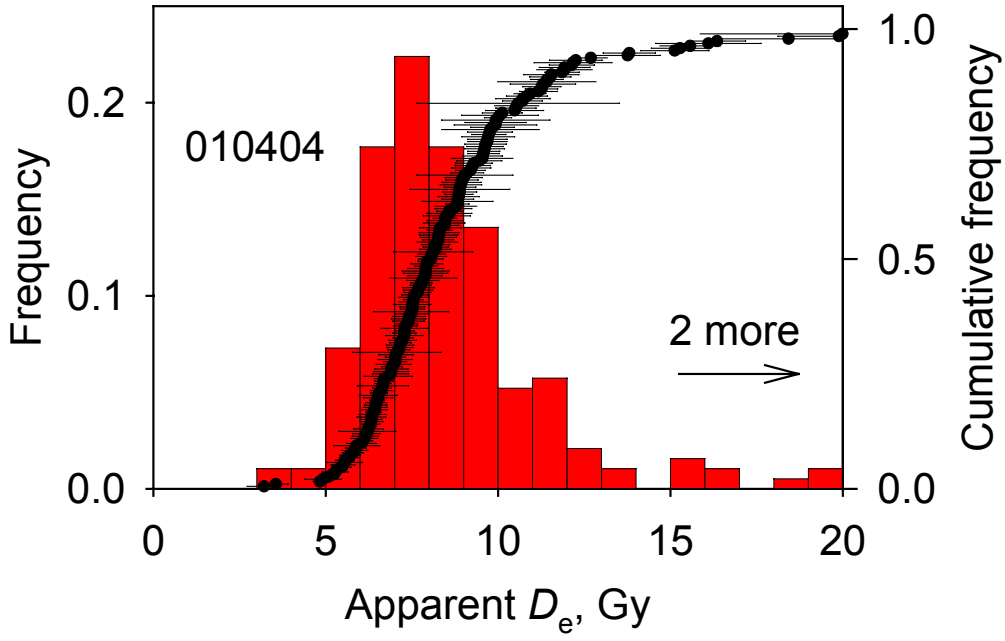

Figure 5.4: The distribution of D_e and the cumulative frequency plot for a sample of sediment from inside the wall (010404, section #2, cf. section 3.2). The figure shows the results of measuring 192 aliquots.

The first sample, 010404, was taken from sediment from within the wall (Figure 5.4). The mean value for the dose distribution is 8.67(21) Gy for 192 aliquots. This value is not the same the peak of the distribution found from the plot. The bottom limit of the dose range is about 5 Gy and the upper limit about 15 Gy; above 15 Gy there are only a few aliquots with large uncertainties. The dose distribution is clearly wider then the dose distribution from the sand above the hearth shown on Figure 5.3, suggesting that this infill sample is less well bleached than the aeolian sand.

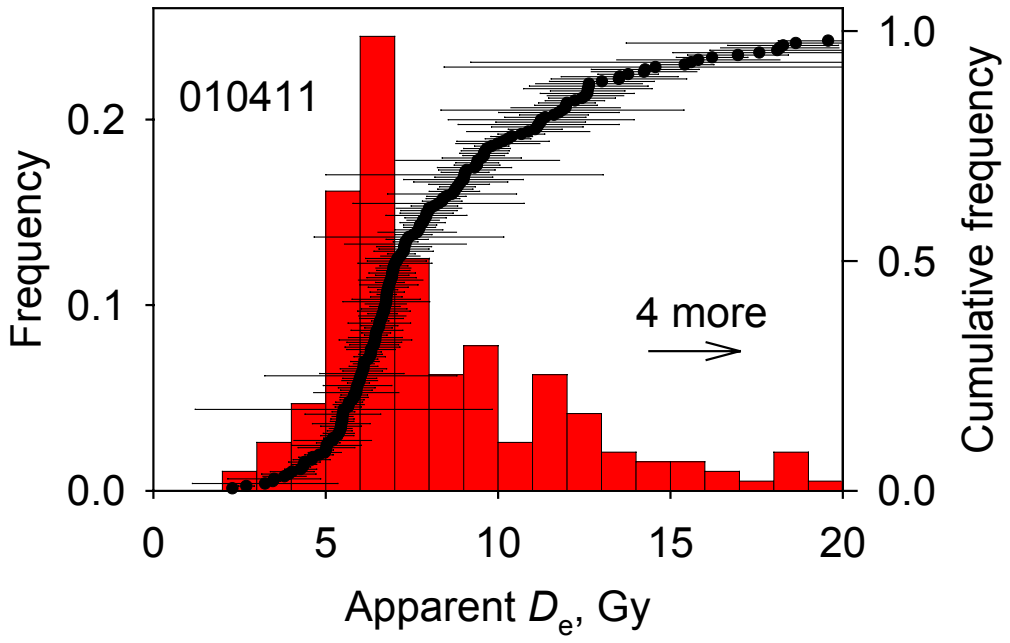

Figure 5.5: The distribution D_e and the cumulative frequency plot for a sediment from within the clearance cairn (010411). The figure shows the results of measuring 192 aliquots.

Results for the sample shown in Figure 5.5 are for sediment from within the cairn. This distribution has a well defined lower limit with only few aliquots having doses less than 5 Gy. The upper range of the distribution is about 13 Gy, but this boundary is poorly defined, as the distribution falls off slowly towards higher doses. The major part of the dose distribution is between 5 and 8 Gy.

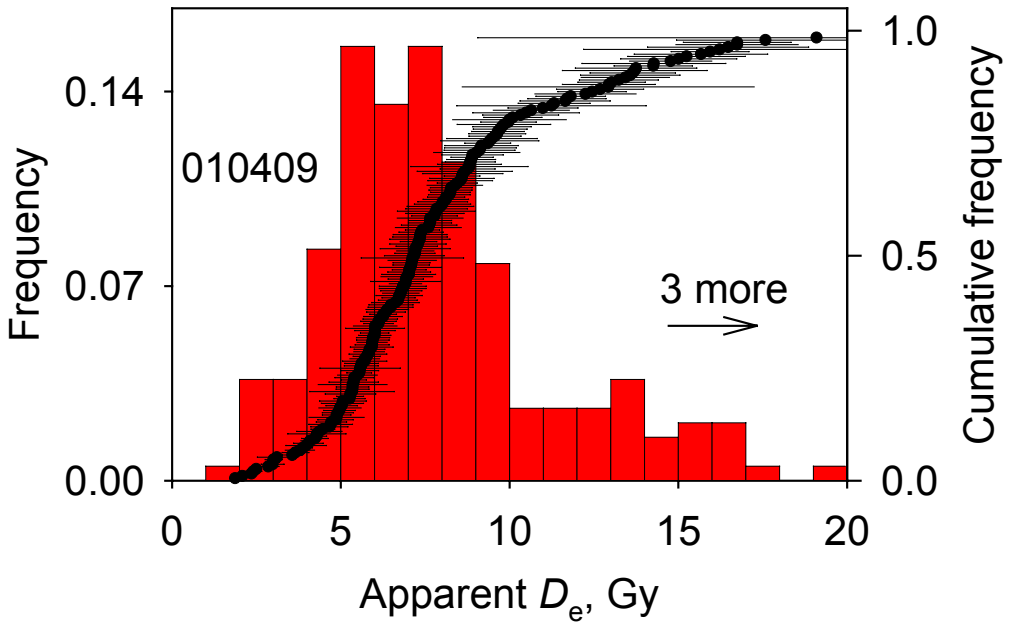

Figure 5.6: The distribution of D_e and the cumulative frequency plot for a sample of sediment from within the wall 010409 (cross section #4). The figure shows the results of measuring 192 aliquots.

Figure 5.6 shows the results from another wall infill sample 010409 (section #4). This dose distribution clearly shows a larger spread in doses than the one found from sample 010411 (Figure 5.5); the majority of the doses fall in the range from 4 to 10 Gy; the peak of the distribution is also not so marked and there is a larger number of aliquots with doses smaller than 4 Gy. These points are well known (estimated uncertainties of about 10%).

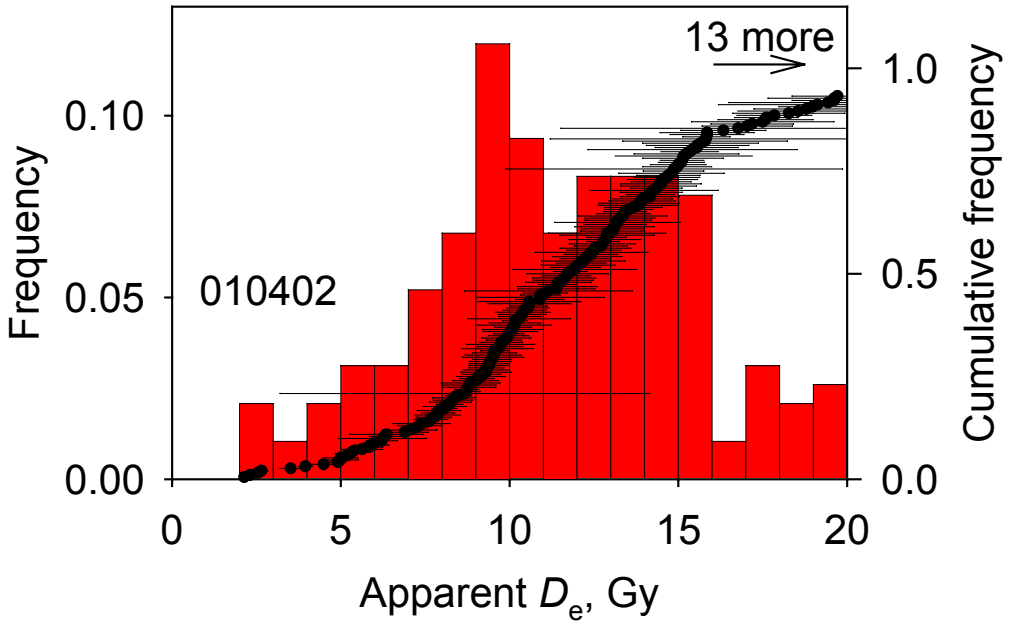

Figure 5.7: The distribution of D_e and the cumulative frequency plot for a sample of sediment from within the wall 010402 (cross section #1). The figure shows the results of measuring 192 aliquots.

Figure 5.7 shows the results for another wall infill sample, 010402. This dose distribution is much broader, and unlike the previous plots the highest point of the distribution is poorly defined. In the range of values from 2 to 6 Gy, the measurements have small uncertainty. The dose distribution increases slowly from a lower limit of around 2 Gy. From the frequency function, one notice that points of high precision are found around 5 and 6 Gy; the largest density of points, however, is found around a dose of 10 Gy, where the shape of the frequency function is steep. At 10 Gy there is also a large variation in the uncertainties.

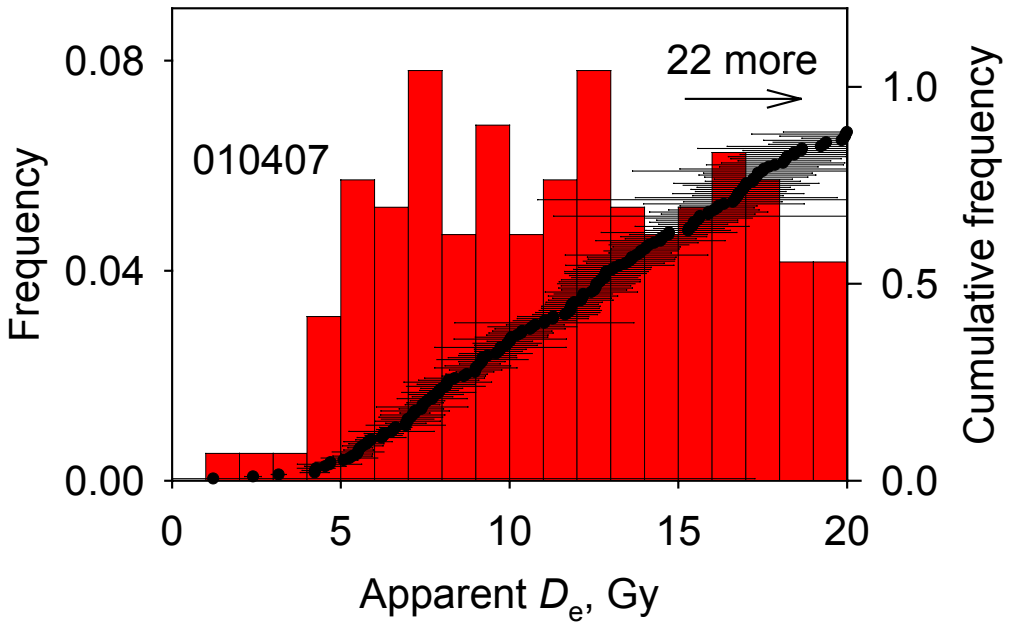

Figure 5.8: The distribution of D_e and the cumulative frequency plot for a sample of sediment from within the wall 010407 (wall cross section #3). The figure shows the results of measuring 192 aliquots.

The results presented on Figure 5.8 are from the last of the five samples taken from material inside the wall. The distribution shows some of the same characteristics as the distributions already presented: there is clear lower limit of the dose distribution around 4 Gy, there are few aliquots with doses between 1 and 4 Gy, but these points have small uncertainties. However, the distribution is very broad and poorly defined; there is no distinct peak. There are also 22 measurements, exceeding 20 Gy. The mean value is 13.59(57) Gy.

5.1.4 Sand below a hearth

An additional sample was taken from the sand below the hearth. It was assumed that this sample would be similar to those samples taken from soil beneath and the stone structures; that is, it was expected that this sample would have a well defined dose distribution with a few aliquots containing small doses, but with greater variation in the upper dose region.

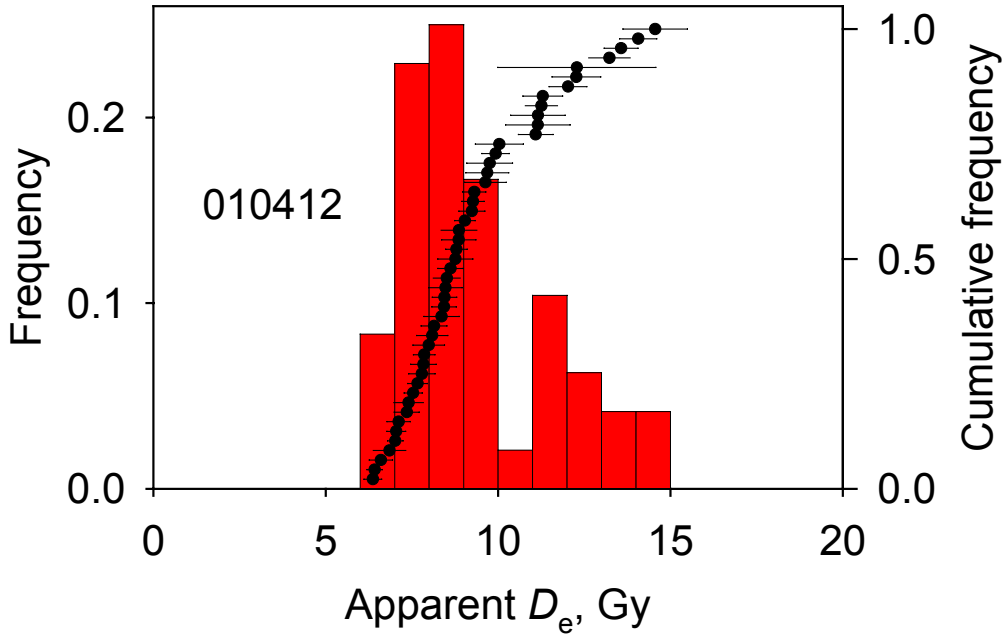

Figure 5.9: The distribution of D_e and the cumulative frequency plot for a sample taken beneath the hearth (fireplace) (010412). The figure shows the results of measuring 48 aliquots.

The measured dose distribution from the sandy soil beneath the fireplace is shown in Figure 5.9. There are no high doses, but there are two separate peaks in the dose distribution, one around 7 Gy and the other around 13 Gy, suggesting that this deposit my not be well-bleached.

5.1.5 Soil beneath the stone structures

Assuming that the stone structures were built directly on topsoil, it can be expected that the smaller doses found in the soil from *beneath* stone structures should be similar to the values found using the sediment from within the stone structures (after allowing for the differences in dosimetry).

Figure 5.10-5.13 shows the results for four soil samples taken from beneath the stone structures at Öggestorp.

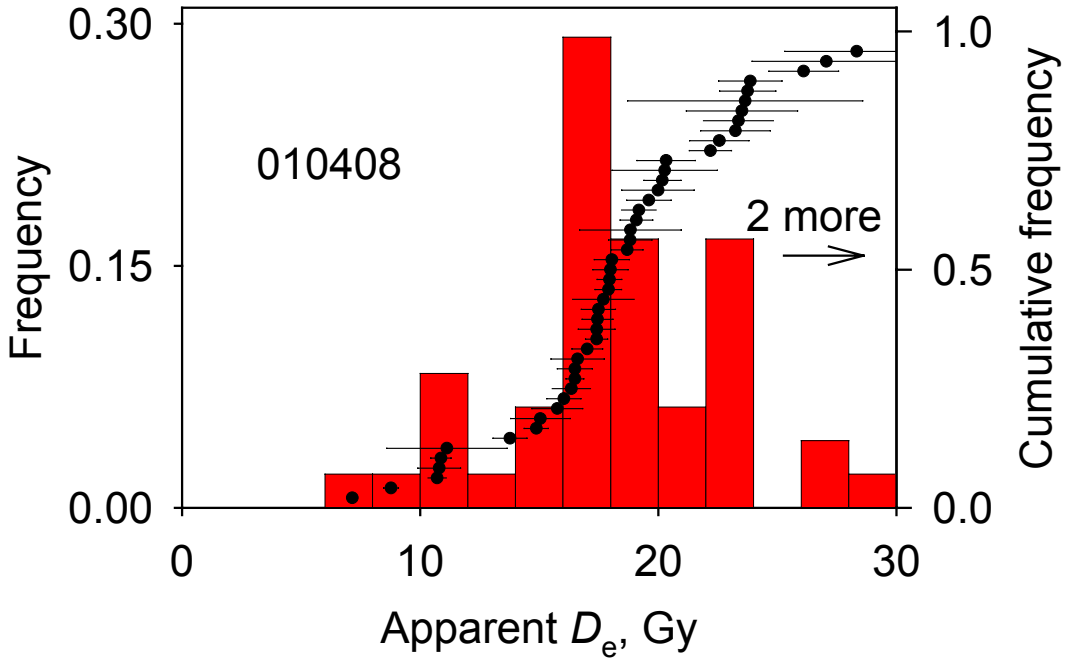

Figure 5.10: The distribution of D_e and the cumulative frequency plot for soil sample 010408 (section #4) taken beneath the wall. The figure shows the results of measuring 48 aliquots.

The D_e distribution for the sample 010408 (section #4) is shown in Figure 5.10. The histogram shows a main peak around 17 Gy as well as a few cases of smaller equivalent doses. The full range of the distribution is between 8 and 30 Gy. But looking on the cumulative frequency it could be noticed that on the histogram there are two more groups of aliquots, the density of points are larger than in the surrounding, one group is about 12 Gy, the other in the range of larger D_e – about 24 Gy.

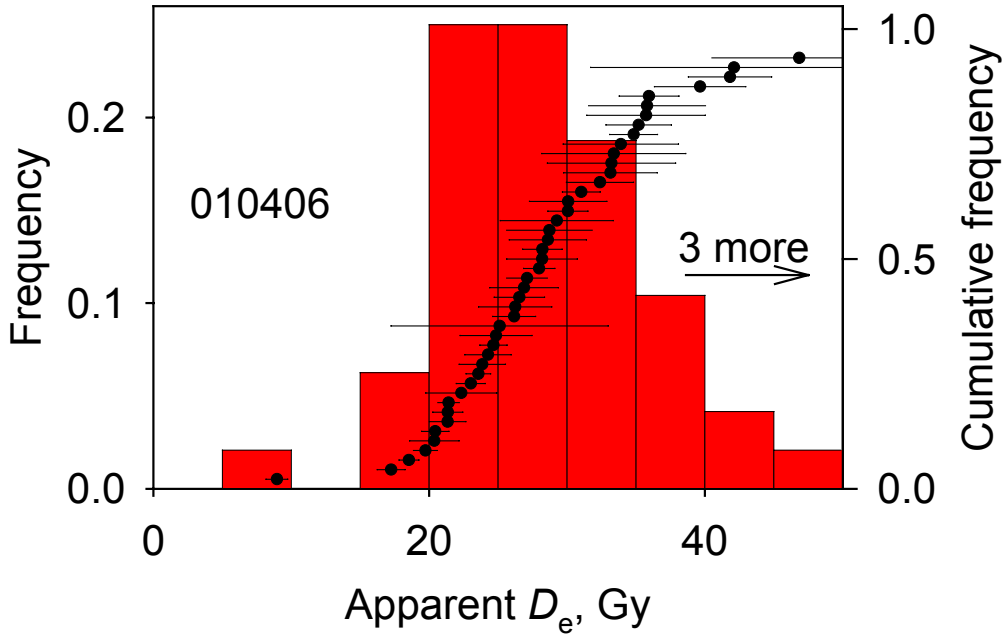

Figure 5.11: The distribution of D_e and the cumulative frequency plot for soil sample 010406 (section #3) taken beneath the wall. The figure shows the results of measuring 48 aliquots.

Figure 5.11 shows the results from another soil sample 010406 taken under the wall (section #3). The dose distribution shows only one aliquot with D_e around 10 Gy and three less then 20 Gy. All these points are not measured very precisely. The peak of this distribution is between 20 to 30 Gy.

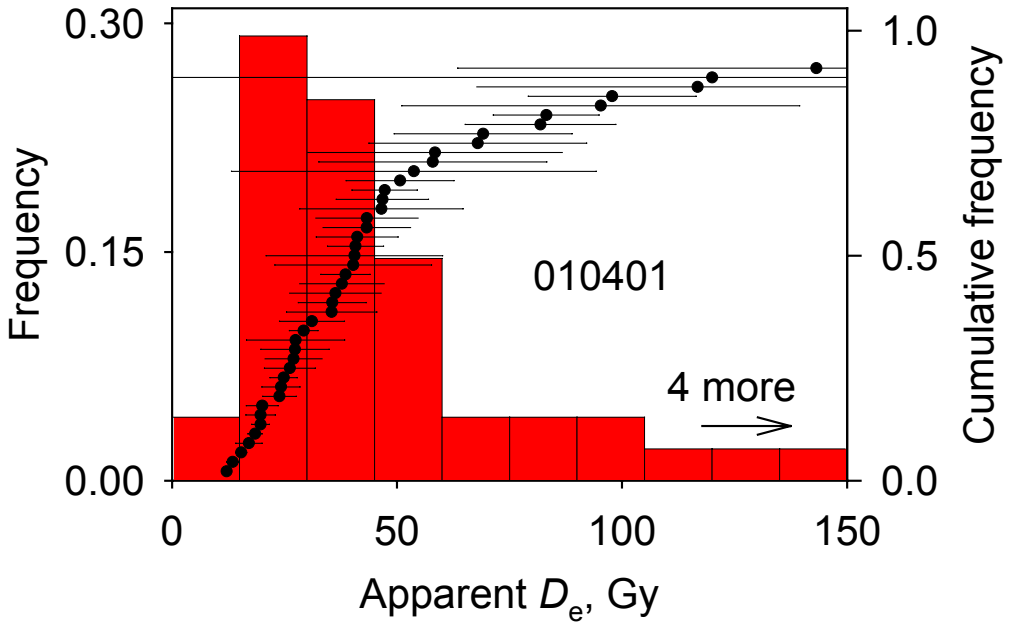

Figure 5.12: The distribution of D_e and the cumulative frequency plot for soil sample 010401 (section #1) taken beneath the wall. The figure shows the results of measuring 48 aliquots.

The third soil sample 010401 is shown on Figure 5.12. This sample is also poorly bleached. Almost all the doses are poorly known; there are only five aliquots with good precision (uncertainties better than 10%), and all these have equivalent doses less then 20 Gy.

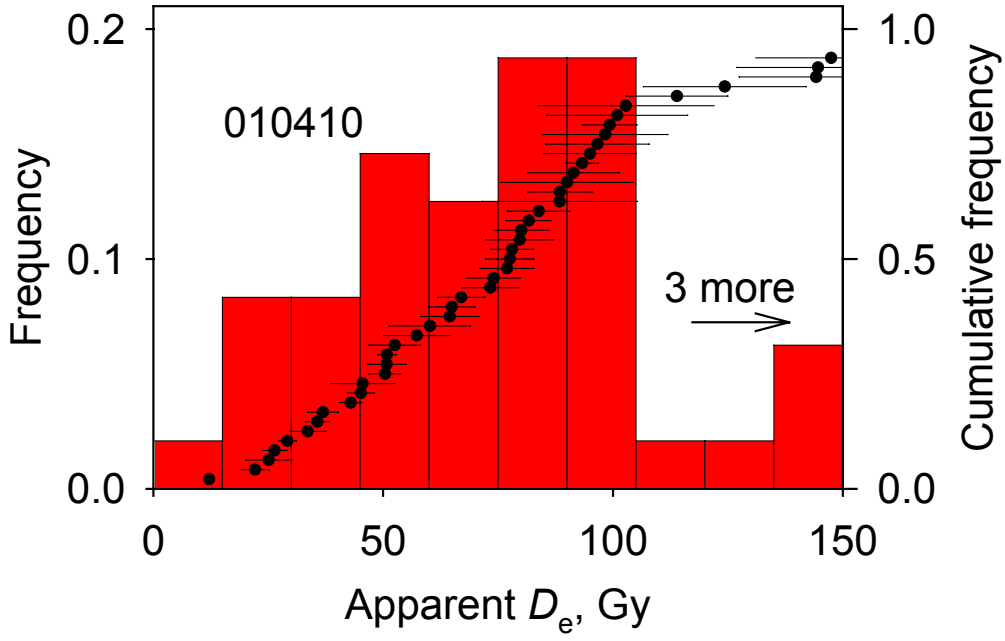

Figure 5.13: The distribution of D_e and the cumulative frequency plot for soil sample 010410, taken beneath the cairn. The figure shows the results of measuring 48 aliquots.

Figure 5.13 shows the final soil sample, taken from under the clearance cairn. Due to high feldspar contamination (cf. Appendix A) a higher cut-heat temperature (220°C) was used during these measurements. Only high equivalent doses were observed using this sample, almost all outside the likely the region of interest of between 8 and 15 Gy (based on an expected age of about 2000 years, and the dosimetry of Chapter 7).

5.1.6 Conclusions

Dose distributions were measured for two modern analogues of the samples from the Öggestorp site: one was sediment infill (Figure 5.1) taken from between bricks from a building demolished in the last 10 years; the second was from topsoil (Figure 5.2) assumed to be similar to that sampled from beneath the stone structures. The infill sample was clearly not well bleached although there were a few well bleached aliquots; the main dose range covering 0.15 to 9 Gy with a few measurements showing an even bigger apparent dose. The topsoil sample was much better bleached; the dose range covering the area between 0 to 2 Gy with a mean value of 0.821(51) Gy.

The sample taken from the sand above the hearth (Figure 5.3) proved to be apparently well bleached, with a mean dose of 5.32(11) Gy. Since this material capped a hearth assumed to be associated with the agricultural period, this dose probably reflects a minimum age for the hearth and thus the agricultural features.

Four sediment infill samples from different location in the stone wall and one sample from within the clearance cairn were studied (Figures 5.4-5.8). Infill sample 010404 (wall section #2; Figure 5.4) shows the most symmetric dose distribution and has a relatively well-defined lower dose limit of about 5 Gy, with only a few results lower then this. Similar results were made for samples 010407 (wall section #3; Figure 5.8), 010409 (wall section #4; Figure 5.6) and 010411 (the clearance cairn; Figure 5.5); these samples also have a relatively well defined lower limit of about 4 to 5 Gy with only a few aliquots having smaller apparent doses. For the last sample 010402 (wall section #1; Figure 5.7) the dose distribution is much less well defined at the smallest doses; only a few aliquots are found in the range around 5 Gy, and the lower limit of these distributions is below 2 Gy.

A sand soil sample was also taken from beneath the hearth. This sample proved not to be as well bleached as the material above the hearth (cf. Figure 5.9).

A final set of four soil samples was taken from underneath the stone structures (Figure 5.10-5.13). The dose distribution found for soil sample 010408 (wall cross section # 4; Figure 5.10) shows some similarity with sediment infill sample 010409 (wall cross section #4; Figure 5.6); these data were sampled at the same cross-section of the wall; both samples have a maximum in the equivalent doses at around 6 Gy but also have some larger values of D_e. The agreement indicates that both samples yield the same time for the building of the wall after the converting the apparent D_e to the ages (cf. Chapter 7). The dose distributions for the remaining three soil samples cover a wide dose range, with maximum values as high as 150 Gy. There are very few aliquots with equivalent doses less then 20 Gy. These samples are poorly bleached and probably cannot be interpreted using the Small Aliquot Regenerative dose method.

5.2 The Single Grain Method

When using the Single Grain method to measure apparent doses, one measures the luminescence from only one grain at a time. For the present measurements the Risø single-grain attachment was used with a 532 nm laser for stimulation [Duller, 2000] and the Single-Aliquot Regenerative-dose (SAR) sequence described in section 4.2. The grain size used for the single grain measurements was 212-250 μm; this grain is dictated by the holes in the sample discs used to present the grains to the reader.

Since it is very difficult to generalize the behaviour and character of individual grains of quartz, tests to determine the most appropriate measurement conditions are difficult to undertaken; usually each grain is different. For simplicity, it was decided to use similar measurement conditions to those used with the single-aliquots described previously: a preheat temperature (the temperature after irradiation of the regeneration dose) of 200°C, and a cut-heat temperature (the temperature after irradiation of the test dose) of 160°C. The lower value of preheat was chosen to be sure that any thermal transfer problems were minimised. Because of the low light levels from the individual grains, the recycling point test was measured by repeating the second (larger) regeneration dose, which is approximately equal to the expected apparent dose.

5.2.1 Results

The Single Grain method was used to measure the apparent doses of the material inside the stone structures and the sand above the hearth. An uncertainty of 10% of the measured dose was added to the calculated uncertainty on each of the equivalent dose measurements. This additional measurement error is based on the observations of Thomsen *et al.* (2002) who have shown that even in ideal conditions, one is not able to measure the equivalent dose in grains of quartz irradiated with a known dose to better than 10%.

5.2.1.1 Aeolian sand above hearth

The aeolian sand was used to illustrate the distribution expected from a well bleached sample. The mean value of dose distribution derived from the single grain measurements (Figure 5.14) is 5.74(20) Gy. The distribution of apparent doses measured using the single grain and single aliquots (Figure 5.3) are similar.

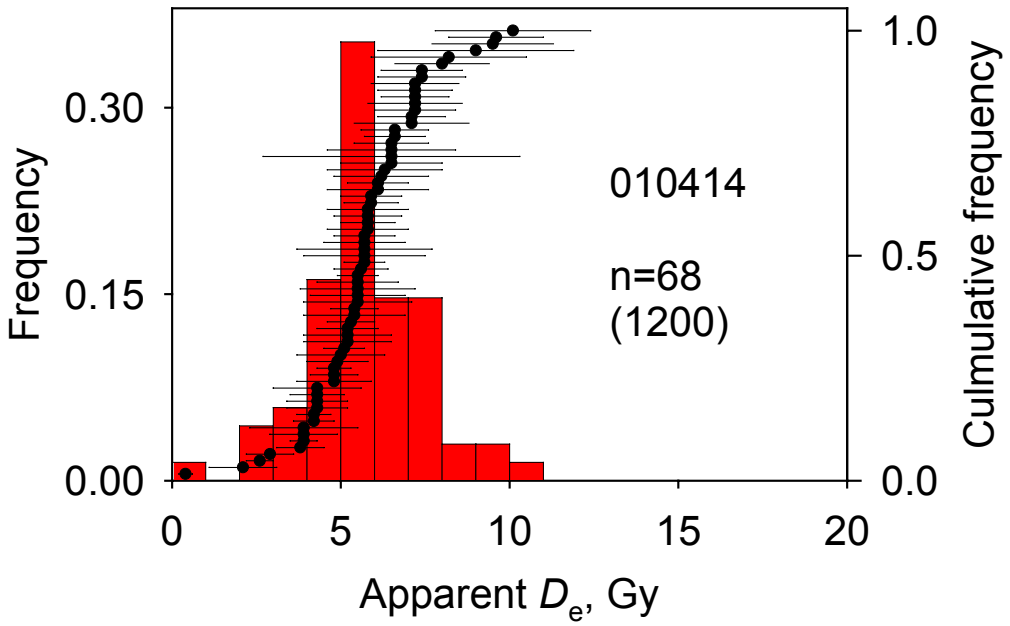

Figure 5.14: The distribution of D_e and the cumulative frequency plot for individual quartz grains from the aeolian sand sample from above the hearth 010414. The figure shows the results of measuring 68 out of 1200 measured grains.

5.2.1.2 Sediment from inside stone structures

5 sediment samples were studied using the Single Grain method, four taken from inside the wall and one from the clearance cairn. The samples studied were the same as those studied using the Single Aliquot approach (cf. section 5.1.3). The results are shown in Figure 5.15-19 and are discussed below.

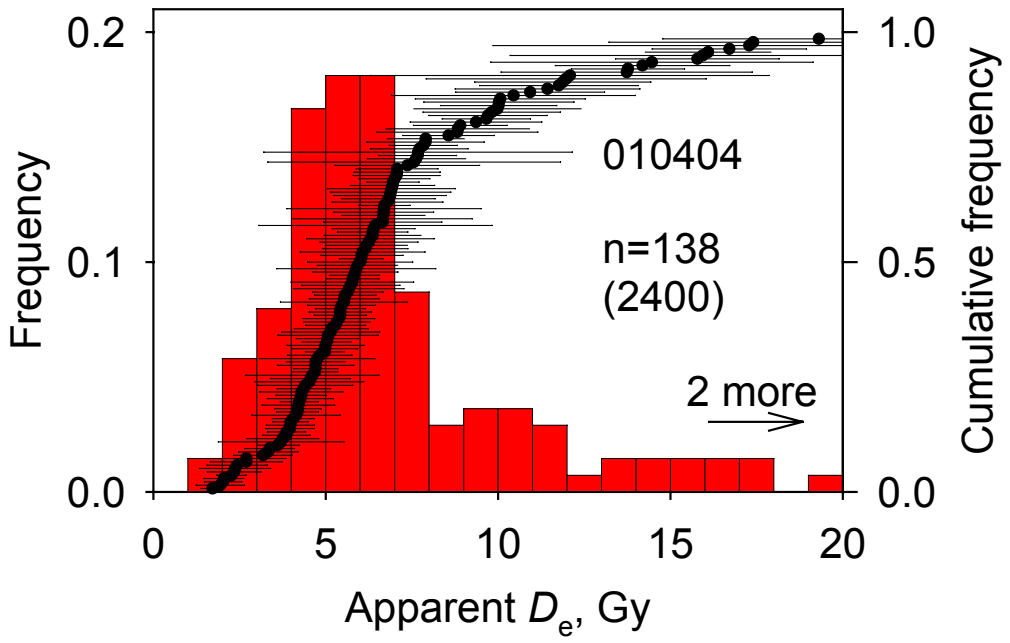

Figure 5.15: The distribution of D_e and the cumulative frequency plot for quartz grains from sediment sample 010404 taken from inside the wall (section #2). The figure shows the results of measuring 138 out of 2400 measured grains.

Figure 5.15 shows the dose distribution found for sample 010404 taken from inside the wall. This distribution is similar to that found using the single aliquot (cf. Figure 5.4). The lower limit is probably between 2 and 3 Gy. The peak of the distribution is in the range from 4 to 7 Gy. There are also aliquots with the D_e larger than 7 Gy, their distribution is rather uniform what could suggest that this infill material was only partially bleached during the later historical event.

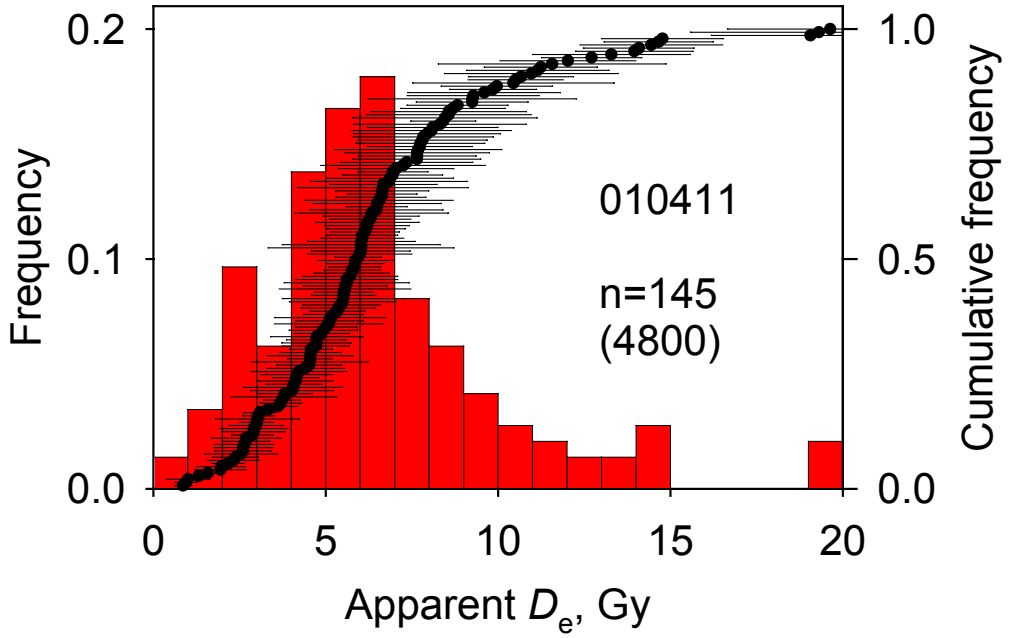

Figure 5.16: The distribution of D_e and the cumulative frequency plot for quartz grains from sediment 010411 taken from the clearance cairn. The figure shows the results of measuring 145 out of 4800 measured grains.

The dose distribution for sample 010411, taken from the clearance cairn, is presented on Figure 5.16. It is somewhat broader than the two distributions already presented, but nevertheless is broadly similar. It is also similar to the single aliquot dose distributions. The lower dose limit is about 3 Gy; four grains have doses smaller than 3 Gy, but their uncertainties are about 25%.

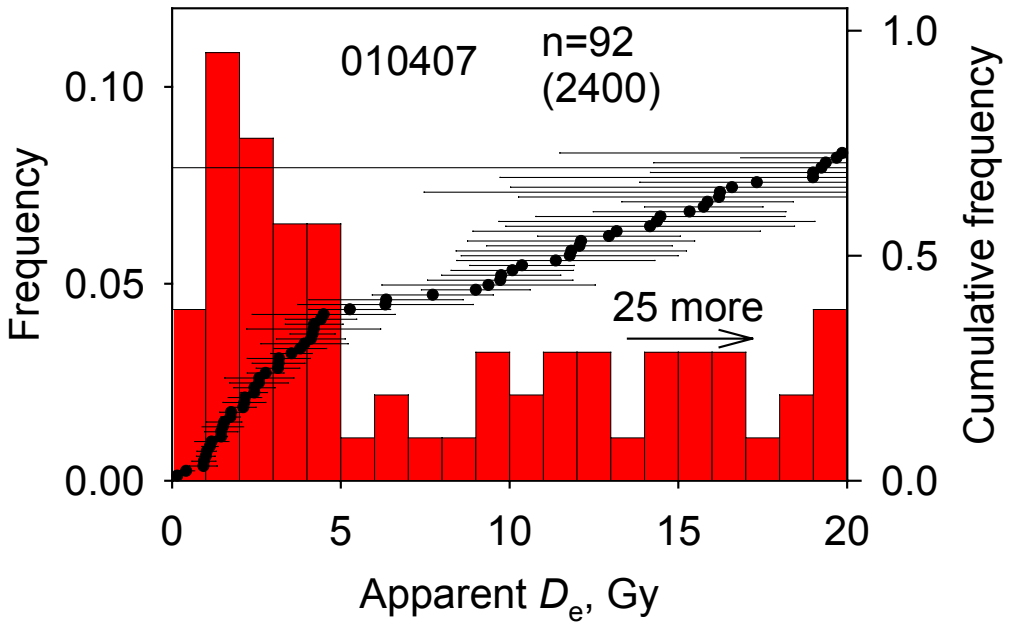

Figure 5.17: The distribution of D_e and the cumulative frequency plot for quartz grains from sediment 010407, taken from inside the wall (section #3). The figure shows the results of measuring 92 out of 2400 measured grains.

The D_e distribution for sample 010407 (Figure 5.17) has a well-defined peak in the low dose region of the distribution, which is otherwise very broad. This peak lies between 0 and 5 Gy, where uncertainties are also fairly small (~12%). No useful information in this range of apparent doses could be extracted using the Single Aliquot approach (Figure 5.8); this is presence of "contaminating" grains, with doses 10 times bigger than the lower (well bleached) grains. Single aliquot results are averaged over all the grains including the partially bleached ones.

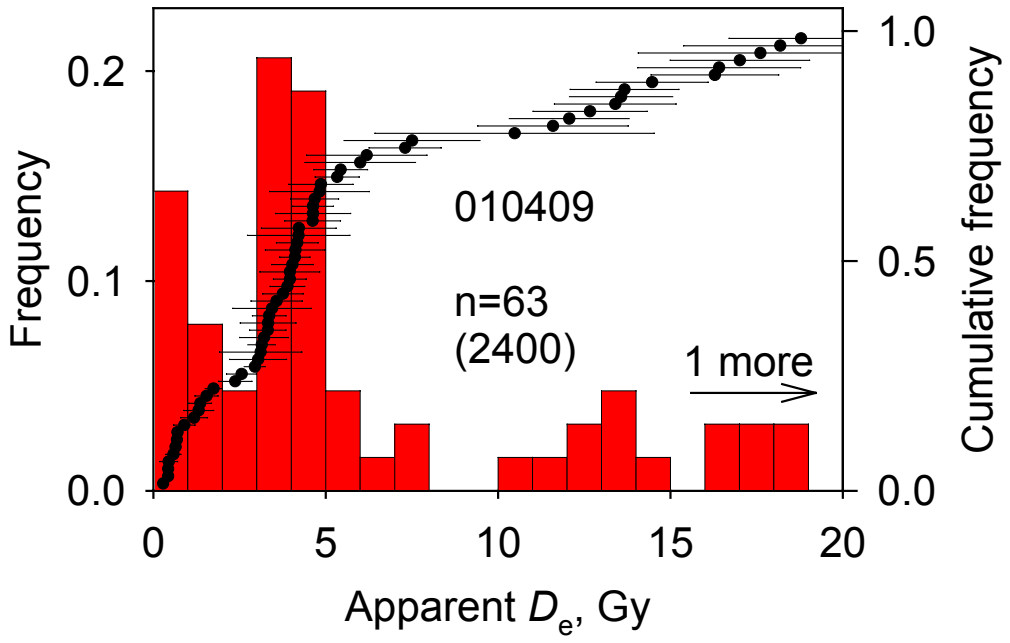

Figure 5.18: The distribution of D_e and the cumulative frequency plot for quartz grains from sediment 010409, taken from inside the wall (section #4). The figure shows the results of measuring 63 out of 2400 measured grains.

Sample 010409 (Figure 5.18) has an interesting and unique distribution of D_e; at least three groups of grains can be identified. One group has low doses, in the range 0 to 2 Gy, one group has doses in the range of 3 to 5 Gy and one group with much higher doses, around 13 Gy. The details of this distribution were not so evident from the single aliquot data (see Figure 5.6), because of dose averaging.

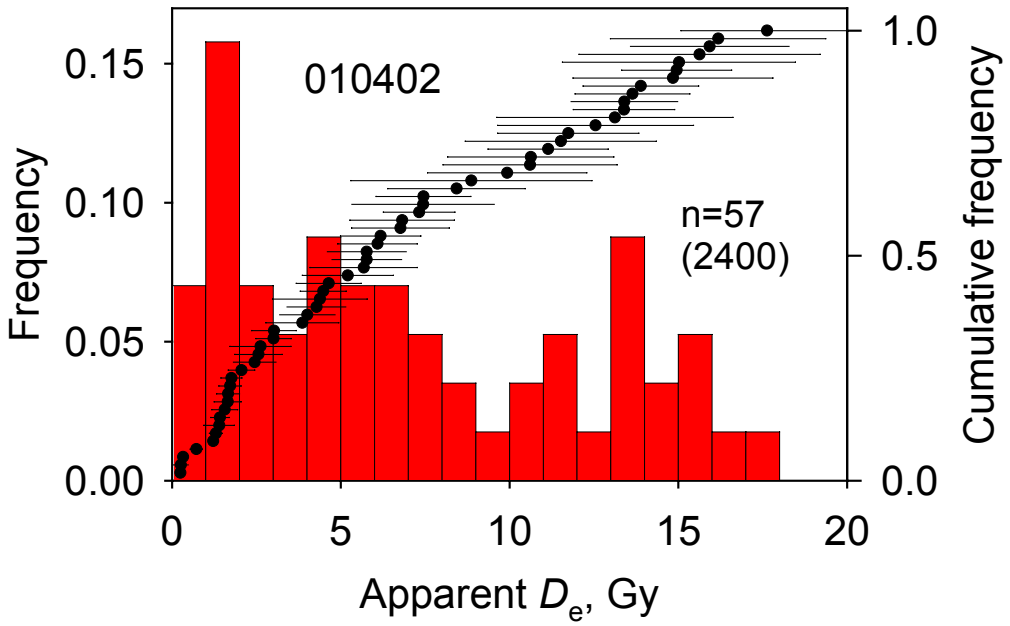

Figure 5.19: The distribution of D_e and the cumulative frequency plot for infill sample 010402 taken from the stone wall (section #1). The figure shows the results of measuring 57 out of 2400 measured grains.

Figure 5.19 illustrates the last sample (010402) studied using the Single Grain approach. This distribution shows at least two groups of grains. The first group has doses around 1 Gy and the second doses around 15 Gy. There may be a third group with doses around 5 Gy, but this is not well defined. This distribution is similar to the dose distribution from sample 010407; both samples show well defined peaks in the dose distributions between 0 and 5 Gy.

5.2.2 Conclusions

Comparing the Small Aliquot and the Single Grain data from sediment inside stone structures, an upper limit of around 12-16 Gy was found to be common for all data sets. This suggests that the sediment making up the infill from the stone structures was completely bleached at some time corresponding to this dose range. This is the earliest evidence of bleaching.

Six samples were studied using both the Single Aliquot and the Single Grain methods. Five samples were taken from inside stone structures (from 4 different cross sections in the wall and from the clearance cairn); the last one was taken from the aeolian sand above the hearth. Three samples show good agreement between the results found using the two different methods, sample 010404 (wall structure – section #2), sample 010411 (clearance cairn) and the aeolian sand sample, presumably because they were all well-bleached at deposition, and so averaging does not obscure important detail in the dose distributions. Furthermore, the infill samples from the wall (010402 section #1) and the clearance cairn (010411) and the sediment sample 010409 (wall structure – section #4) have similar doses to that found in the aeolian sand; in all these data sets groups of grains are identified with apparent doses around 4-6 Gy.

Infill samples from the wall 010402 (section #1), 010407 (section #3) and 010409 (section #4) all display groups of grains having doses in the range between 0 and 3 Gy. These groups were not so evident from the single aliquots data. The presence of two separate “peaks” in the apparent dose distribution in the range of 0 to 1 Gy and from 3 to 4 Gy suggests that the lower peak belongs to at least one additional bleaching event, such as rebuilding or expansion of the “old” wall, or perhaps some other event, such as deposition of wind-blown sand during an unusually stormy and dry period. In the dose distributions of the infill samples 010402 and 010407, identifiable peaks are only observed for apparent doses in the 0 to 3 Gy range; the measurements in the range of 4 to 5 Gy have too big uncertainties to be reliably identified as a separate event. This lends weight to the suggestion that the corresponding bleaching event was related to construction, rather than storms; the latter could not have removed the older dose signature, but only added to it.

6 Dose distribution in heated material using small aliquots

This chapter reports the results of OSL measurements on heated material. Unlike the measurements presented in Chapter 5, these samples are expected to be well zeroed, as they were thermally reset during the heating process. Two samples were studied, both heated stone samples. The first sample is from the hearth (010413), the other from the wall (010405 – section #2). They were measured using the Single Aliquots method and the SAR protocol, described in detail in Chapter 4.

6.1 Introduction

The heated stones were found in the hearth and in the stone wall (section #2), respectively. On the assumption that the wall section containing the heated stone is built only shortly after the stone was heated, the age of the heated stone and the unheated sediment sampled from within the wall section should be the same. Hence, the heated stone found in the wall was expected to give an independent estimate of the time of building for this section of stone wall. The other heated stone found in the hearth was expected to give independent support to the age of the overlying aeolian sand, and of the general period of human agricultural activity in the area.

6.2 Heated sample taken from inside the wall

The dose distribution illustrated on Figure 6.1 shows the measured doses from sample 010405 (stone wall – section #2). The mean value is 12.77(19) Gy and in good agreement with the peak of the distribution. This is to be expected from a well zeroed sample: the dose distribution is narrow and approximately normally distributed. The uncertainties on the measurements are also relatively small; this is not surprising, because it is well-known that heating can sensitise quartz by orders of magnitude.

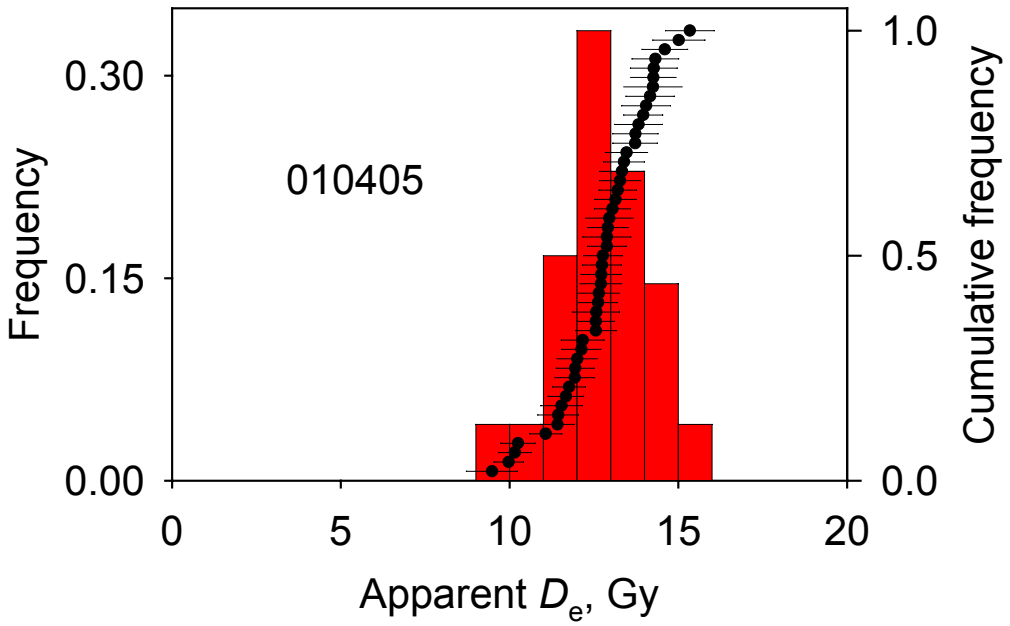

Figure 6.1: The distribution of D_e and the cumulative frequency plot for a heated stone sample from inside the wall structure (010405 - section #2). The figure shows the results of measuring 48 aliquots.

6.3 Heated sample taken from the hearth

Figure 6.2 shows the result of measuring the apparent doses from a sample stone found in the hearth (010413). The dose distribution is very narrow, and the mean value yields a very precise estimate of D_e, of 2.919(18) Gy. As for the sample from the heated stone inside the wall, the uncertainties on the measured apparent doses from the hearth are small, again confirming the heating of this stone in the past.

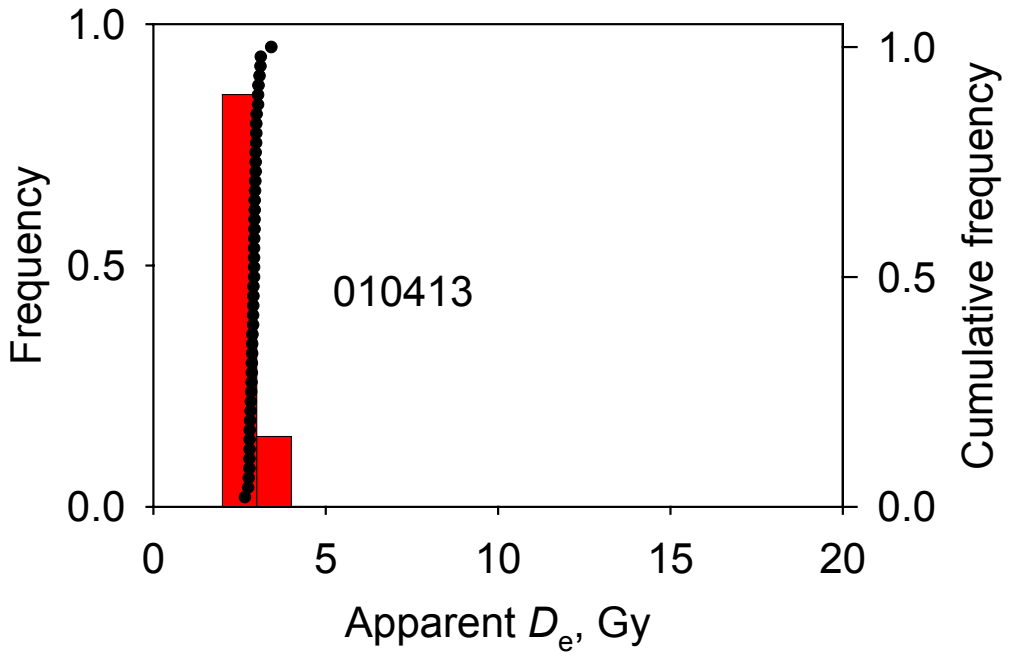

Figure 6.2: The distribution of D_e and the cumulative frequency plot for a heated stone sample from the hearth (010413). The figure shows the results of measuring 48 aliquots.

6.4 Conclusion

Since the measurements from both of the samples taken from heated stones has a very small uncertainty, it seems likely that these samples should yield reliable information on the dating of the Öggestorp archaeological site. It should be noted, though, the material taken from the heated stones found in the wall and the hearth, have different properties than the infill or soil samples. It is also interesting to note that the mean doses for the two heated stones are very different. Without dose rate information, one cannot tell if these two stones were heated at the same time or not.

7 Dose rate measurements

In this chapter the dose rates measured on material found at the archaeological site in Öggestorp are discussed. Information on the dose rates is essential for determining the ages of the sediments and stones presented in the earlier chapters.

7.1 Natural radiation

The natural ionising radiation present in the environment originates mainly from the decay of the natural radionuclides including ^{232}Th, ^{238}U, ^{235}U and ^{40}K, and a smaller fraction from cosmic rays. These radioactive isotopes are naturally present in the crust, and are left from the earth's formation. Other "new" radionuclides have been introduced to the environment by human activity, these radionuclides have never been in sufficient concentrations to contribute significantly to environmental dose rates, except in very unusual circumstances. They can safely be ignored in this study. When the natural long-lived radioisotopes of uranium and thorium decay they give rise to further "daughter nuclides", which are also radioactive. The activity of these radionuclides is supported by the parent decay, and so they are said to be in secular equilibrium. Different types of decay processes and hence different types of radiation contribute to the natural radiation environment. The heaviest of the emitted particles are the alpha particles. They have the greatest mass and ionise materials strongly. The range of penetration of material is quite short, only up to a few tens of μm in quartz. The two other types of radiation do not ionise materials so densely, but they have a much greater penetration depth, for beta particles it is up to 3 mm and for gamma radiation up to 0.3 m.

Another source of natural radiation *cosmic rays* has two components close to Earth's surface, one called "soft" and the other "hard", because of their different penetration characteristics [Szczeniowski, 1974]. The "soft" component constitutes the largest part of cosmic radiation at sea level. This component is absorbed by the material relatively easily (in about half a metre of sediment). The "hard" component has a very low probability of ionising material (not easily absorbed by material and have a great penetrating depth).

The intensity of the cosmic rays at Earth's surface depends on the latitude, the altitude, the depth and the density of the material studied. Dependence on the latitude and altitude is due to the magnetic fields around the Earth and influences the "soft" component the most.

Quartz does not contain significant radioactivity within the crystal structure, and because of the short range of alpha radiation, external alpha contributions are removed during the HF acid treatment used to etch the outside of the grain. This leaves only the core, irradiated almost entirely by beta and gamma radiation, and cosmic rays.

Radiation *dose* is in general defined as the energy absorbed per unit mass. In the SI system, the unit of the dose is 1 Gy = 1 J/kg. The rate of absorption of radiation by a material is called the *dose rate*. The SI unit is 1 Gy/s.

7.2 The age equation

The half-lives of the parent radionuclides responsible for the majority of the natural radiation flux (uranium, thorium, and potassium) lie in the range 10^8-10^{10} years. For comparison, the age of galaxy is in the range of 10^{11} years. Consequently, the decay of these radionuclides is so small that it may be considered constant through historical times. Thus the total dose accumulated over time is proportional to the dose rate and time:

$$D = d \cdot t$$

where d is the dose per year, t is time in years.

The OSL method uses the information on total dose (i.e. the equivalent dose, D_e) and the assumption of a constant annual dose rate, d, to determine the time, t, since the last bleaching event of a sample.

The dose rate necessary to determine the OSL age may be measured using several techniques. It could be measured by placing a sensitive artificial radiation dosimeter for some period of time in the place, where a sample was taken. Another possibility is to perform measurements of gamma and beta radiation on a sample in the laboratory.

The effective dose rate may again be derived from:

$$d_{ef} = f \cdot d_{\beta} + d_{\gamma} + d_{c}$$

where f is the attenuation factor for the beta contribution for a fixed grain size (in the present experiments the grain size was 180-250 μm, and $f = 0.89$), and d_{β}, d_{γ}, d_{c} are the effective dose rates for beta, gamma and cosmic radiation, respectively. The effective dose rates for each type of radiation are calculated as follows:

$$d_{p} = \frac{d_{pd}}{1 + H_{r} \cdot W}$$

where d_{p} is the effective dose rate for one type of radiation, d_{pd} is the dose rate for one type of radiation for a dry sample, H_{r} is a constant which is 1.25 for beta, 1.14 for gamma, and W is defined as

$$W = \frac{w_{w} - w_{d}}{w_{d}}$$

w_{w} – is the weight of a water saturated sample, and w_{d} is the weight of the same sample when dry.

The presence of water in the natural environment must be taken into account because it can significantly attenuate the total dose rate. An increase in water content of about 1% decreases the dose rate (and so increases age) by about 1%.

The water content is always estimated by measuring the *natural mass*, the *saturation mass* and the *dry mass*. The natural mass is a measure of the weight of a sample before it comes into the laboratory. Afterwards, this sample is heated at 60°C until the weight is constant, this is the dry mass. The saturation mass is measured by adding water until the sample is not able to take any more water. One then needs to estimate the average percentage of saturation from knowledge of the site characteristics, and climate. For the

southern Sweden, and samples taken about 1 m below the soil surface, the samples were probably close to saturation for their entire burial period.

7.3 Results

Risø no.	*Description*	*Sample type*	*^{238}U Bq/kg*	*^{226}Ra Bq/kg*	*^{232}Th Bq/kg*	*^{40}K Bq/kg*
010401	Wall #1, west face soil	Soil	26.3(5.2)	30.00(0.91)	32.03(0.80)	699(28)
010401A	Wall #1, west face soil	stone	13.9(3.5)	14.06(0.58)	19.67(0.53)	491(20)
010402	Wall #1, west face infill	sediment	26.6(4.7)	27.98(85)	22.26(68)	661(27)
010402A	Wall #1, west face infill	stone	27.7(3.9)	26.43(66)	55.10(83)	1260(41)
010403	Wall #2, south face soil	Soil	26.5(5.2)	23.38(89)	25.53(77)	746(31)
010403A	Wall #2, south face soil	stone	23.2(3.5)	19.17(58)	28.47(58)	719(26)
010404	Wall #2, south face infill	sediment	30.6(5.5)	37.1(1.0)	28.64(80)	681(29)
010404A	Wall #2, south face infill	stone	24.3(3.8)	28.88(71)	16.84(52)	450(19)
010405	Wall #2, south face stone	heated stone	49.4(6.9)	38.43(60)	88.62(94)	2045(37)
010406	Wall #3, west face soil	Soil	38.1(5.7)	36.9(1.0)	28.01(82)	640(28)
010406A	Wall #3, west face soil	stone	16.2(3.9)	20.60(67)	28.60(64)	699(26)
010407	Wall #3, west face infill	sediment	23.5(7.0)	42.36(1.3)	24.03(96)	572(29)
010407A	Wall #3, west face infill	stone	42.1(4.9)	30.48(46)	25.09(40)	1025(19)
010408	Wall #4, east face soil	Soil	34.5(4.9)	31.62(87)	29.96(74)	784(30)
010408A	Wall #4, east face soil	stone	25.5(4.5)	22.64(76)	27.34(69)	800(30)
010409	Wall #4, east face infill	sediment	35.4(7.7)	30.57(64)	31.18(60)	731(16)
010409A	Wall #4, east face infill	stone	21.4(4.2)	20.88(70)	32.95(71)	756(28)
010410	A981 Cairn, north face soil	Soil	21.5(5.8)	28.2(1.0)	26.03(84)	671(30)
010410A	A981 Cairn, north face soil	stone	28.3(3.8)	28.01(66)	36.67(66)	955(32)
010411	A981 Cairn, north face infill	sediment	30.8(7.8)	46.85(75)	30.88(58)	699(15)
010411A	A981 Cairn, north face infill	stone	14.9(7.6)	18.8(1.2)	29.0(1.1)	829(38)
010412	A97, below fireplace	sediment	28.0(6.5)	26.7(1.1)	20.11(88)	722(34)
010413	A97, fireplace, stone	heated stone	12.2(2.9)	9.93(48)	8.65(38)	106.1(8.7)
010414	A97, above fireplace	sediment	37.7(5.1)	29.86(89)	20.97(69)	664(27)

Table 6: Radionuclides concentrations.

Dose rates were measured for each sample separately, because the background radiation can vary significantly with location. For each sample a radiation spectrum was measured using high-resolution gamma spectroscopy [Murray *at all*., 1987], to give concentrations of the ^{238}U, ^{232}Th series, and ^{40}K. Dry dose rates were calculated from these concentration using the tables [Olley *at al*., 1996]. Radionuclides concentrations were measured for material taken from around each sampling location, including infill material

and adjacent stones. The results are summarised in Table 6 along with the dry beta and gamma dose rates derived from the infill and stones samples.

It is important to consider the construction of the stone structures. Detailed information about the proportion and the position of stones and infill material is not available, although sampling location were chosen in such a way that the infill sediment from the cavity at least 10 cm diameter, and at least 1 cm from the nearest stone. Hence, it can be reliably assumed that the beta dose rate originates only with the sediment. The gamma dose rate originates from both the sediment and from the surrounding stones; it was assumed that 50(15)% of the dose rate derived from sediment, and also from the surrounding stones. The infill material accumulated in the spaces between the stones through time. This process must have led to a time dependence in the dose rate. But assuming an uncertainty 15% in the gamma dose, it is assumed that this variation has been included in the uncertainty. The beta dose rate is unaffected by this process.

It is also important to consider the heated stones. For the sample taken from the heated stone in the wall, the beta dose rate is derived only from the heated stone; the gamma dose rate is assumed to derive 50(15)% from the sediment and 50(15)% from the heated stone. For the sample taken from the heated stone from hearth, the beta dose rate is also derived from the sample; the gamma dose rate is derived 75(15)% from the sand below and above the hearth and 25(15)% from the heated stone (because there are no other adjacent stones, unlike in the wall). For the soil samples from under the wall and cairn, the beta dose rate was derived from the sediment and the 50(15)% of the gamma dose rate from the sediment and 50(15)% from the stone. The results for the total dose rates and water contamination are shown in Table 7:

Risø no.	*Description*	*w.c. %*	*Dry dose rate from sediment, Gy/ka*		*Dry dose rate from stone, Gy/ka*		*Total dose rate, Gy/ka*
			beta	*gamma*	*beta*	*gamma*	
010401	Wall #1, west face soil	13	2.18(10)	1.162(34)	1.460(70)	0.731(20)	3.01(21)
010402	Wall #1, west face infill	21	2.017(96)	1.00(32)	3.70(16)	1.86(40)	2.99(18)
010403	Wall #2, south face soil	18	2.22(11)	1.074(32)	2.140(95)	1.058(27)	2.74(11)
010404	Wall #2, south face infill	29	2.17(10)	1.156(40)	1.460(69)	0.780(29)	2.472(87)
010405	Wall #2, south face stone	0			5.99(22)	2.987(45)	7.46(38)
010406	Wall #3, west face soil	33	2.10(10)	1.117(39)	2.071(94)	1.051(28)	2.54(14)
010407	Wall #3, west face infill	44	1.87(10)	1.047(43)	3.00(11)	1.343(30)	2.33(12)

Risø no.	*Description*	*w.c. %*	*Dry dose rate from sediment, Gy/ka*		*Dry dose rate from stone, Gy/ka*		*Total dose rate, Gy/ka*
			beta	*gamma*	*beta*	*gamma*	
010408	Wall #4, east face soil	26	2.42(11)	1.218(36)	2.36(11)	1.134(31)	2.89(11)
010409	Wall #4, east face infill	29	2.294(91)	1.183(29)	2.26(10)	1.134(29)	2.760(86)
010410	A981 Cairn, north face soil	17	2.05(10)	1.52(34)	2.84(12)	1.408(35)	2.83(14)
010411	A981 Cairn, north face infill	33	2.282(91)	1.265(42)	2.38(13)	1.145(35)	2.701(76)
010412	A97 sand below hearth	36	2.15(11)	1.011(36)			2.261(70)
010413	A97 hearth, stone	0			0.417(29)	0.263(12)	1.216(91)
040114	A97 sand above hearth	30	2.071(97)	1.002(34)			2.321(75)

Table 7: Water content, dry dose rates and total effective dose rates. Activity concentrations have been converted to dry dose rates using the factors given by [Olley *et al.*, 1996].

The total dose rates shown in Table 7 was corrected for the small internal quartz dose rate of 0.06(3) Gy/ka as well as the cosmic ray dose rate, which was calculated from the equation given by Prescott *et all*. [1994]; for infill and soil samples the cosmic ray dose rate is 0.1835(92) Gy/ka, for the hearth samples (heated stone, sand below and above) it is 0.1690(85) Gy/ka.

8 Discussion and conclusion

The aim of this thesis was to demonstrate the possibility of using OSL measurements as a new and absolute method to date stone structures in an archaeological context. Indeed, this offers many new possibilities for modern archaeology. Some of the existing dating methods were listed in Table 1 (Chapter 3). In general, most dating methods involve comparison with historical artefacts found on or near the place/ site of interest. Another method of dating is the ^{14}C (radiocarbon) method, which allows dating of organic findings, including charcoals and bones (human or animal). Organic material, however, is not always present. One such case is stone structures.

At the Jönköping site, charcoal was often found inside the stone structures, and this has been using the radiocarbon method. The ages obtained were in general much younger than the expected age, and very variable. This has been explained as arising from the use of fire to stimulate growing grass for grazing (cf. section 3.1), as the area has been mainly an agriculture area.

During the sampling, charcoal was also found in the hearth (fireplace). It was dated by radiocarbon to 1.99(7) ka (including an additional 52 years to correct for AD 2002 [L. Häggström, 2002]). The charcoal was burnt in the fireplace and then covered by subsequent sand deposition. It was almost certainly 'in situ' when sampled, and so the dating of the charcoal may be trusted. It is regarded as an independent age estimate for this site.

Three new age estimates have been derived from the data presented in this thesis. The data originating from OSL measurements on two heated stones and the aeolian sand above the hearth are discussed in Chapter 5 and Chapter 6. The ages found are 2.40(20) ka for the heated stone from the hearth; 1.71(11) ka for the heated stone from the wall (section #2) and 2.29(13) ka for the aeolian sand above the hearth. These ages are in good agreement with each other, and with the ^{14}C age from the hearth. These data help to define at least one period when the wall and cairn were constructed.

Comparing the dose distributions derived using single aliquots and single grains, respectively, one concludes that the result for the aeolian sand is the same regardless of the method. The results for samples 010404 (Figure 5.4 and Figure 5.15) and 010411 (Figure 5.5 and Figure 5.16) are also consistent with those above; the age found for the lower limit of both samples is about 2 ka [Baran, in press].

For the remaining samples, which are clearly only partially bleached, it proves more difficult to obtain a reliable age estimate, especially when considering the single aliquots results; in most cases it is impossible to determine a peak in the relevant region of the distributions. The lower doses aliquots yield an age of about 1 ka. These inconsistency is solved by turning to the single grain measurements, which provide more information on bleaching of the samples. For sample 010407 (Figure 5.17 for single grain) the lower limit yields an age of about 0.6 ka. For samples 010409 (Figure 5.18) and 010402 (Figure 5.19) the lower limits yield values about 0.3 ka; there was clearly a relative recent bleaching event is the history of the wall. But there is probably another event at 2 ka recorded in the single grain data for these samples, presumably the same as that recorded by the heated stones, ^{14}C data, and the well-bleached samples (cf. Appendix B).

To conclude, this study has demonstrated the potential of using OSL techniques to date sediments inside agricultural stone structures such walls and cairns. Using the single aliquot data, some information is obscured by averaging in particular that connected with the smallest doses (ages). Most of the information discussed above has come from the single grain measurements, as the soil dated by the single aliquot method proved very difficult to interpret; usually resulting in overestimates the equivalent doses.

9 References

1. Aitken M. J. (1998) "An Introduction to Optical Dating". Oxford University Press, Oxford.

2. Baran J., Murray A. S., Häggström L. "Estimating the age of stone structures using OSL: the potential of entrapped sediment" submitted to Quaternary Science Reviews (Quaternary Geochronology).

3. Bluszcz A. (2000) "Datowanie luminescencyjne osadów czwartorzędowych – teoria, ograniczenia, problemy interpretacyjne". Politechnika Śląska, *Zeszyty Naukowe* **Nr 1434**, Gliwice.

4. Bøtter-Jensen L., Bulur E., Duller G. A. T., Murray A. S. (2000) "Advances in luminescence instrument systems". *Radiation Measurements* **32**, 523-528.

5. Duller G. A. T., Murray A. S. (2000) "Luminescence dating of sediments using individual mineral grains". *Geologos* **5.**

6. Duller G. A. T., Bøtter-Jensen L., Murray A. S. (2000) "Optical dating of single sand-sized grains of quartz: sources of variability" *Radiation Measurements* **32**,453-457.

7. Häggström, L. (2002) *private communication*.

8. Murray A. S., Marten R., Johnston A., Martin P. (1987) "Analysis for naturally occurring radionuclides at environmental concentrations by gamma spectrometry". *Journal Radioanalytical Nuclear Chemistry*, Articles **115**, 263-288.

9. Murray A. S., Olley J. M., Caitcheon G. C. (1995) "Measurement of the equivalent doses in quartz from contemporary water-lain sediments using optically stimulated luminescence". *Quaternary Science Reviews (Quaternary Geochronology)* **14**, 365-371.

10. Murray A. S., Wintle A. G. (2000) "Luminescence dating of quartz using an improved single-aliquot regenerative-dose protocol". *Radiation Measurement* **32**, 57-73.

11. Olley J. M., Murray A. S., Roberts R. G. (1996) "The effects of disequilibria in the uranium and thorium decay on burial dose rates in fluvial sediments". *Quaternary Science Reviews (Quaternary Geochronology)* **17**, 1033-1040.

12. Olley J. M., Caitcheon G. G., Roberts R. G. (1999) " The origin of dose distributions in fluvial sediments, and the prospect of dating single grains from fluvial deposits using optically stimulated luminescence". *Radiation Measurements* **30**, 207-217.

13. Prescott J. R., Hutton J. T.(1994) "Cosmic ray contributions to dose rates for luminescence and ESR dating large depths and long-term time variations". *Radiation Measurement* **23**, 497-500.

14. Szczeniowski Sz. (1974) "Fizyka doświadczalna" Część VI – "Fizyka jądra i cząstek elementarnych". PWN, Warszawa.

15. Thomsen K. J., Murray A. S., Bøtter-Jensen L. (2002) "Controls on the Distribution of Measured Doses in Single Grains of Quartz". 24-28 of July, 2002, Conference in Reno, USA.

16. Wallinga J. (2002) "On the detection of OSL age overestimation using single-aliquot techniques". *Geochronometria* **21**, 17-26

Appendix A Chemical preparation of samples

When working with samples for luminescence dating in the laboratory, they must be protected from the influence of daylight. Usually, the samples arrive in black plastic bags to protect them during the transportation. All steps of the chemical preparation are subsequently made in the dark room with only orange light present. The protection from daylight is of course necessary in order to avoid that the signals collected by the samples are lost.

Before any chemical treatment, a sample is sieved to extract suitable grains for luminescence dating. Afterwards, the desired grain size is treated by HCL and H_2O_2 to remove all carbonates and organic material, in the chemical reaction. Following this treatment samples are usually free of any carbonates or organic material. They may then safely be treated with concentrated HF acid to remove feldspar and etch the quartz surface, which may otherwise complicate the dosimetry. Only the core of the grain is left. Residual feldspar contamination is checked by tests using infrared (IR) stimulation. The quartz grains do not give any luminescence signal during the IR stimulation.

The 180 to 250 μm grains for the four soil samples 010401, 010403, 010410, and 010412 needed to be treated by HF acid twice. Only two of them, however, were afterwards “clean”; samples 010403 and 010410 still contained feldspars. These samples were etched three times by concentrated HF acid. Even so, one of them (010410) could only be dated using the higher cut-heat temperature of 220°, as the feldspars were still giving a significant IR signal after the normal cut-heat temperature (160°C). The other sample (010403) was not dated at all due to the high contamination of feldspars.

Groups of grains of different sizes were chemically cleaned for three samples (010402, 010404, 010411), the grains studied were in the range 90 to 1000 μm: 90-180 μm, 250-300 μm, 300-500 μm and 500-1000 μm. Only the smaller grains were cleaned once as they did not give any IR signal. The larger grains (>500 μm) needed to be etched at least twice. Two samples, 010402 and 010411, were etched three times and still gave a significant IR signal. Also, the number of grains in the samples decreased dramatically with each etching.

Usually, the grains disintegrated into a mixture of small and large grains. To preserve the right grain size, the samples were thus sieved again after the etching.

Appendix B The ages of chosen groups of aliquots and grains

The table below shows average values of D_e in ranges, which were pointed out in the text of this thesis and recalculated to ages.

Symbol of a sample	*Method*	*Material*	*Range D_e, Gy*	*n*	*Average D_e, Gy*	*Age, ka*
010405 F.6.1	single aliquot	heated stone	all	48	12.77(19)	1.71(11)
010413 F.6.2	single aliquot	heated stone	all	48	2.919(18)	2.40(20)
010414 F.5.3	single aliquot	aeolian sand	all	48	5.32(11)	2.29(13)
010402 F.5.7	single aliquot	infill	~2	3	2.34(12)	0.782(69)
			9-11	54	10.30(12)	3.44(25)
010404 F.5.4	single aliquot	infill	5-10	151	7.67(10)	3.10(17)
010407 F.5.8	single aliquot	infill	1-4	3	2.26(56)	0.97(25)
			4-5	17	5.15(14)	2.21(15)
010409 F.5.6	single aliquot	infill	<4	15	3.00(17)	1.086(82)
			4-10	123	6.86(13)	2.48(13)
010411 F.5.5	single aliquot	infill	5-8	115	6.687(94)	2.47(12)
010414 F.5.14	single grain	aeolian sand	all	68	5.74(20)	2.47(16)
010402 F.5.19	single grain	infill	<2	13	1.17(16)	0.391(60)
			4-6	9	4.91(23)	1.64(14)
			13-16	11	14.54(33)	4.86(37)
010404 F.5.15	single grain	infill	2-3	19	3.13(17)	1.26(10)
			4-7	85	5.83(12)	2.36(13)

Symbol of a sample	*Method*	*Material*	*Range D_e, Gy*	*n*	*Average D_e, Gy*	*Age, ka*
010407 F.5.17	single grain	infill	0-5	34	2.41(22)	0.92(11)
010409 F.5.18	single grain	infill	0-2	14	0.88(13)	0.318(50)
			3-5	26	3.89(12)	1.408(83)
			~13	5	13.56(29)	4.91(27)
010411 F.5.16	single grain	infill	<2	5	1.14(13)	0.421(52)
			2-3	25	2.90(11)	1.072(65)
			4-7	70	5.55(10)	2.05(10)
010401 F.5.12	single aliquot	soil	<20	8	17.0(1.1)	5.64(56)
010406 F.5.11	single aliquot	soil	~10	1	8.96(79)	3.53(72)
			10-20	3	18.50(72)	7.3(1.4)
			20-30	24	25.02(58)	9.8(1.8)
010408 F.5.10	single aliquot	soil	<10	2	7.96(81)	2.75(54)
			10-12	4	10.878(88)	3.76(70)
			16-20	25	18.13(26)	6.3(1.0)
			22-24	8	23.27(21)	8.0(1.3)
010410 F.5.13	single aliquot	soil	10	1	12.15(69)	4.29(58)
010412 F.5.9	single aliquot	soil	6-10	36	8.25(17)	3.65(21)
			11-15	12	12.33(36)	5.45(33)

Table 7: Ranges of histogram peaks, their averages, number of aliquots in the range and calculated values of OSL ages. Number of the relevant figure is given directly under the symbol of the sample.